AD NUMBER

AD901763

NEW LIMITATION CHANGE

TO

Approved for public release, distribution unlimited

FROM

Distribution authorized to U.S. Gov't. agencies only; Proprietary Information; APR 1971. Other requests shall be referred to Naval Undersea Research and Development Center, San Diego, CA 92132.

AUTHORITY

NUC D/N ltr, 5 Aug 1974

NUC TP 294

UNDERSEA DETECTION OF VARIOUS SIGNALS

edited by
A. Gordon
Ocean Technology Department

July 1972

NAVAL UNDERSEA RESEARCH AND DEVELOPMENT CENTER, SAN DIEGO, CA. 92132

AN ACTIVITY OF THE NAVAL MATERIAL COMMAND

CHARLES B. BISHOP, Capt., USN
Commander

Wm. B. McLEAN, Ph.D.
Technical Director

ADMINISTRATIVE INFORMATION

The Naval Undersea Research and Development Center has been tasked by Naval Ship Systems Command, PMS 395, to reconsider the relative merits of various physical phenomena that are capable of underwater information transfer. The work in this publication is the final report on this task.

Work was performed from September 1970 to March 1971 under project S-1001, Task S-1001-001.

ACKNOWLEDGMENTS

The editor gratefully acknowledges the contributions of the various section authors and also the advice and assistance of Ivor Lemaire and Don Moore.

Released by
I. P. LEMAIRE, Head
Advanced Systems Division

Under authority of
H. R. TALKINGTON, Head
Ocean Technology Department

SUMMARY

PROBLEM

Discuss, in a form suitable for comparison, the most important characteristics of underwater information-transfer methods. This information should help designers interested in underwater communications, navigation, detection, and identification.

RESULTS

1. Tradeoffs involved in the undersea detection of static and time-varying signals were examined, and quantitative results were obtained.

2. Static electric and magnetic fields, radioactive fields, chemical systems, extremely-low-frequency (ELF) electromagnetic radiation, light, and acoustics were studied, and the results were summarized in chart form.

3. For time-varying fields, underwater light exhibits inferior range and ELF exhibits inferior bandwidth when compared with acoustics.

4. When used as static markers, ranges to approximately 3 and 14 km can be achieved for chemical and ELF sources, respectively.

5. Considerations beyond the preliminary design stage are not discussed in this report, and more detailed treatises, many of which are referenced, should be consulted.

CONTENTS

GLOSSARY

A – ampere
Å – angstrom
Ci – Curie
cm – centimeter
cpm – cycles per meter
dB – decibel
deg – degree
eV – electronvolt
ft – feet
G – gauss
g – gram
H – henry
hr – hour
Hz – hertz
in. – inch
J – joule
keV – kiloelectronvolt
kg – kilogram
kHz – kilohertz
km – kilometer
l – liter
lb – pound
m – meter
MeV – megaelectronvolt
mg – milligram
mi – mile
min – minute
MHz – megahertz
ml – milliliter
mm – millimeter
MW – megawatt
N – Newton
Oe – oersted
rad – radian
sec – second
V – volt
μW – microwatt

INTRODUCTION

To those who are accustomed to air as the supporting or propagating medium, the underwater transfer of information presents new problems: In the ocean environment, some standard information-transferring techniques which are used in the atmosphere are nearly useless, and other techniques which are inappropriate in a gaseous environment perform well. For example, high-frequency electromagnetic radiation, the most widely used information carrier on land, is severely attenuated in conducting seawater; acoustic propagation, however, exhibits lower attenuation in the sea than in the air.

The purpose of this report is to discuss, in a form suitable for comparison, the various techniques that are useful in the underwater transfer of information. As information transfer is fundamental to problems of underwater markers, communication, navigation, detection, and identification, it is hoped that the comparisons in this report will be useful to a wide variety of investigators who are unfamiliar with the special limitations of the ocean environment. Although the various contributors have not given an exhaustive account of their subjects, it is believed that there is sufficient information for the reader to evaluate the tradeoffs involved, for example, in choosing a particular mode of marking a given location or devising an underwater navigation system.

Section I is a series of charts which present the tradeoffs involved in various methods of underwater information transfer or site marking. (The charts are in an extremely condensed form.) These charts are self-contained, and can be used without referring to their corresponding texts in Section II. It is strongly recommended, however, that the appropriate text be consulted because some assumptions made by the authors might vary from the specific parameters envisioned for the reader's system. The charts particularly emphasize maximum range for threshold detectability because the background noise, dispersion, and attenuation encountered in the ocean often place severe restrictions on the usable range. The ranges on the charts reflect as much as possible the natural environmental limitations on range. Considerations of additional noise created by detection or by insufficient state-of-the-art detection sensitivity are discussed in Section II.

Section II, which contains articles corresponding to the charts in Section I, explains in detail the methods of calculating the values which appear on the charts. In addition, the problems involved in implementing the various methods are discussed. In view of the sponsor's interest in navigation applications, some of the articles are written more directly towards that goal, although much of the material is applicable in other areas. The last article in Section II, necessarily more qualitative than the others and lacking a corresponding chart, reviews undersea mechanical navigation aids.

SECTION I: CHARTS

This section consists of charts which tabulate the tradeoffs between the various methods of underwater marking and information transfer. The juxtaposition of the charts makes comparisons convenient. The charts, however, should be used only in conjunction with their corresponding articles in Section II because the charts are the direct contributions of the various authors and are written from slightly different perspectives.

Some charts were prepared assuming coherent detection, while others assumed incoherent detection. Slight differences in the signal-to-noise-ratio criteria appear among the various authors. The ranges in some of the charts are obtainable with current equipment or techniques, while others are based on what is available in the near term. For these reasons, the charts must be used with care, and the corresponding articles should be read before meaningful comparisons are made.

Chart 1. Static Electric and Magnetic Fields. (See article on page 12.)

Static Magnetic Field

Source	Dimensions	Weight (W)	Power or Magnetization (P or M)	Noise Power Spectrum ($\Phi(K)$)	Range (R)	Effect of Changing Parameters	
Copper torus	$r_1 = 1.00$ m $r_2 = 10^{-1}$ m	2 tons	P = 10 W M = 5.44×10^3 A-m^2	$=[49.6/K\gamma^2 + 7.9\times10^3\gamma^2 m]$	30 m	$R\sim M^{0.370}$ $R\sim P^{0.185}$ $R\sim d^{-0.370}$	$R\sim \bar{I}_{\Phi}^{0.185}$ R~(winding's resistivity)$^{-0.185}$ $R\sim r_1^{0.555}$
Permanent magnet	Length $\gg$ width Volume = 0.25 m^3	2 tons	M = 2.61×10^5 A-m^2	$=[49.6/K\gamma^2 + 7.9\times10^3\gamma^2 m]$	130 m	$R\sim M^{0.370}$ $R\sim d^{-0.370}$ $R\sim \bar{I}_{\Phi}^{0.185}$	$R\sim W^{0.370}$ $R\sim B_r^{0.370}$
Filled solenoid	Length = 2π m Diameter = 0.2 m	3.8 tons	M = 3.2×10^5 A-m^2 P = 70 W	$=[49.6/K\gamma^2 + 7.9\times10^3\gamma^2 m]$	135 m	$R\sim M^{0.370}$ $R\sim d^{-0.370}$ $R\sim \bar{I}_{\Phi}^{0.185}$	$R\sim W^{0.370}$
Superconducting coil	$r_1 = 1.00$ m	-	M = 3.56×10^6 A-m^2	$=[49.6/K\gamma^2 + 7.9\times10^3\gamma^2 m]$	320 m	$R\sim M^{0.370}$ $R\sim d^{-0.370}$ $R\sim \bar{I}_{\Phi}^{0.185}$	$R\sim r_1^{0.555}$

Static Electric Field

Electric dipole	Length = 2π m $r_s = 0.1$ m		P = 10 W	$=[1.29/K + 1.8\ m] \times 10^{-14}$ (V/m)^2	160 m	$R\sim P^{1/6}$ $R\sim d^{-0.330}$ $R\sim \bar{I}_{\Phi}^{0.166}$ $R\sim U^{-0.330}$	$R\sim r_s^{1/6}$ $R\sim l^{1/3}$ $R\sim \sigma^{-1/6}$ $R\sim B_0^{-1/3}$

notes:
- r_1 large radius of torus
- r_2 small radius of torus
- K radian spatial frequency
- d signal-to-noise ratio
- $\bar{I}_{\Phi}$ average of $(\Phi(K))^{-1}$ across signal
- B_r remnant magnetic induction
- B_s saturation magnetic induction
- r_s radius of spherical dipole termination
- σ water conductivity
- U ocean current velocity
- B ambient dc magnetic field
- l transmitter antenna length

Chart 2. Radioactive Fields. (See article on page 26.)

Source	Source's Dimension	Source's Weight	Source's Power	Detector	Sensitivity	Range	Effect of Changing Parameters
^{60}Co	<1-in. cube	Negligible	100 Ci	Scintillation detector	10^{-8}n/hr $10^{-2}\gamma/cm^2/sec$	3 m	$R/R_0 \approx 1n$ Ci, where R_0 = 15.4 cm for ^{60}Co
^{252}Cf	<1-in. cube	Negligible	10^{11} n/sec	BF^3 counter	10^{-3} n/cm^2/sec	2.6 m	20 cm per tenfold increase in intensity
^{252}Cf	<1-in. cube	Negligible	Induced activation in seawater from 10^{11}/sec	Scintillation detector	$10^{-2}\gamma/cm^2/sec$		Dependent on current and dispersion. 1 km for 1-knot current.

Chart 3. Chemical Systems. (See article on page 30.)

Type of Marker	Background	Minimum Detection Limit, D_0	Release Rate, R_0	Amount Required for 1000 hr of Operation	Cost of Material*	Range	Effect of Parameters on Range
Rhodamine B	<0.01 ppb	0.01 ppb	10 g/hr	10 kg	$30/kg	3 km	Range ∝ R_0/D_0
Fluorescein	<0.01 ppb	0.01 ppb	10 g/hr	10 kg	$20/kg	3 km	Range downstream decreases and range upstream increases as current velocity decreases. Total range along current axis remains approximately constant.
Iodine-131	300 pCi/l	30 pCi/l	0.03 Ci/hr	30 Ci	$1200/Ci	3 km	
Iron-59	300 pCi/l	30 pCi/l	0.03 Ci/hr	30 Ci	$28,000/Ci	3 km	
Copper ion	0.003 ppm	0.6 ppm	2.4×10^6 g/hr	2.4×10^6 kg**	$8/kg	3 km	
Mercuric ion	0.03 ppb	2 ppb	2700 g/hr	2700 kg†	$30/kg	3 km	
pH	8.1	±0.1 pH units	3.7×10^4 equivalent/hr (equivalent of H^+ to reduce pH by 0.1 unit)	3.7×10^7 equivalent	$0.01/equivalent	3 km	Lateral range ∝ (current velocity)$^{-1/2}$

*Cost for laboratory grades and quantities.

**Weight of cupric nitrate ($Cu(NO_3)_2 \cdot 3H_2O$).

†Weight of mercuric chloride ($HgCl_2$).

Chart 4. Extremely-Low-Frequency Electromagnetic Waves. (See article on page 42.)

Depth, m	Frequency, Hz	r/δ_w	r/δ_b	T x P x l, J-m	Range, m	Remarks	Effect of Changing Parameters
0	4	90		10^4	11,300	Surface effects included	$r \sim 2.3 \log \frac{N(\omega)}{TPl}$ $r \sim \sigma_w^{-1/2}$
0	10	170		10^4	13,600		
0	100	750		10^4	19,000		
100	4	63		10^4	7900		
100	10	95		10^4	7600		
100	100	70		10^4	1700		
400	4	13.5		10^4	1700	Infinite medium approximation	$r \sim 2.3 \log \frac{N(\omega)}{TPl}$ $r \sim \sigma_w^{-1/2}$
400	10	17		10^4	1360		
800	4	16.3		10^4	2000		
> 1300	4	19		10^4	2400		
> 720	10	20		10^4	1600		
> 180	100	22		10^4	330		
> 1300	4		18	10^4	14,400	Near bottom	$r \sim 2.3 \log \frac{N(\omega)\sigma_w^2}{TPl}$ $r \sim \sigma_b^{-1/2}$
> 720	10		20	10^4	10,400		
> 180	100		21	10^4	3360		

notes:
- r range
- δ_w attenuation length in water
- δ_b attenuation length in seabed
- T observation time, sec
- P transmitter input power, W
- l antenna length, m
- $N(\omega)$ spectral noise power density
- σ_w water conductivity
- σ_b bottom conductivity

Chart 5. Underwater Propagation of Light. (See article on page 66.)

Laser Type	Power Input	Power Output (efficiency)	Attenuation Coefficient (attenuation length)	Depth	Range (limited by)	Effect of Varying Parameters	
Argon ion	10^4 W	10 W (0.1 percent)	0.039/m 26 m	75 to 650 m	610 to 860 m (daylight penetration)	$R \sim \alpha^{-1}$	$\Delta R \sim \frac{1}{\alpha} \ln \frac{P}{P_0}$
						$\Delta R \sim \frac{1}{\alpha} \ln \frac{\sqrt{t}}{\sqrt{t_0}}$	$\Delta R \sim \frac{1}{\alpha} \ln \frac{\sqrt{H_0}}{\sqrt{H}}$
Argon ion	10^4 W	10 W (0.1 percent)	0.039/m 26 m	650 to 4000 m	860 to 1030 m (bioluminescence)	$R \sim \alpha^{-1}$	$\Delta R \sim \frac{1}{\alpha} \ln \frac{P}{P_0}$
						$\Delta R \sim \frac{1}{\alpha} \ln \frac{\sqrt{t}}{\sqrt{t_0}}$	$\Delta R \sim \frac{1}{\alpha} \ln \frac{\sqrt{H_0}}{\sqrt{H}}$
Argon ion	10^4 W	10 W (0.1 percent)	0.039/m 26 m	>4000 m	1030 m (photon limited)	$R \sim \alpha^{-1}$	$\Delta R = \frac{1}{\alpha} \ln \frac{t}{t_0}$
						$\Delta R \sim \frac{1}{\alpha} \ln \frac{\overline{P}}{P_0}$	
Frequency-doubled YAG	500 W	5 W average, 5×10^6 W peak	0.06/m 17 m	75 to 650 m	520 to 690 m (daylight penetration)	$R \sim \alpha^{-1}$	$\Delta R \sim \frac{1}{\alpha} \ln \frac{P}{P_0}$
						$\Delta R \sim \frac{1}{\alpha} \ln \frac{\sqrt{t}}{\sqrt{t_0}}$	$\Delta R \sim \frac{1}{\alpha} \ln \frac{\sqrt{H_0}}{\sqrt{H}}$
Frequency-doubled YAG	500 W	5 W average, 5×10^6 W peak	0.06/m 17 m	650 to2500 m	690 to 710 m (bioluminescence)	$R \sim \alpha^{-1}$	$\Delta R \sim \frac{1}{\alpha} \ln \frac{P}{P_0}$
						$\Delta R \sim \frac{1}{\alpha} \ln \frac{\sqrt{t}}{\sqrt{t_0}}$	$\Delta R \sim \frac{1}{\alpha} \ln \frac{\sqrt{H_0}}{\sqrt{H}}$
Frequency-doubled YAG	500 W	5 W average, 5×10^6 W peak	0.06/m 17 m	>2500 m	710 m (photon limited)	$R \sim \alpha^{-1}$	$\Delta R = \frac{1}{\alpha} \ln \frac{t}{t_0}$
						$\Delta R \sim \frac{1}{\alpha} \ln \frac{\overline{P}}{P_0}$	

notes:
- R range of laser
- α attenuation coefficient
- t_0 observation time used, 5 sec
- t observation time
- P_0 average laser power assumed
- $\overline{P}$ average laser power
- P_0 laser peak power assumed
- P laser peak power
- H_0 background illumination used
- H background illumination

Chart 6. Underwater Acoustic Propagation. (See article on page 78.)

Frequency, kHz	Resolution, m	Noise Level, dB/μbar/Hz		Source Power, W*	Transducer Size, cm**	Attenuation, dB/km	Transmission Loss, dB	Range, km
		Sea State	Thermal					
10	1.0	−71		1000	15	0.98	147.6	54
32	0.56	−79		100	5	8.3	133.1	6.8
100	0.32		−75	10	1.5	31	106.6	1.4
320	0.18		−65	1	0.5	67	74.1	0.35
1000	0.10		−55	0.1	0.15	315	41.6	0.034

*Cavitation limited at 1 W/cm^2.

**1 wavelength diameter.

SECTION II:

ARTICLES

STATIC ELECTRIC AND MAGNETIC FIELDS

by

A. Gordon
NUC

CONTENTS

STATIC ELECTRIC AND MAGNETIC FIELDS

INTRODUCTION

A technique that has been used to detect and locate submerged objects is the observation of their associated electric or magnetic fields. Objects consisting of more than one type of metal usually experience electrolytic decomposition in the sea. The electric field caused by this process is detectable at a distance generally greater than the dimensions of the object being sought. These fields and the objects producing them have been located by towing electrodes from surface vessels, a method which has been used to locate sunken torpedoes, ships, and planes (ref. 1).

Towed magnetometers have also been used to locate submerged objects which are magnetized or magnetizable in the earth's field. This type of object superimposes on the earth's field a short wavelength anomaly that can be detected by the magnetometer. The magnetometer trace of the sunken USS THRESHER is a good example (ref. 2).

The present article is concerned with the detection of various types of static electric and magnetic sources which are located on or near the ocean bottom. It will be assumed that these objects are being searched for with a detector that is also near the bottom, for example, a magnetometer mounted on a towed fish or submersible. The basic questions that this article will address are listed below.

1. What is the maximum range at which an electric or magnetic source can be detected given a set of parameters describing the source and surrounding environment?

2. How does the maximum range change as these parameters are varied?

In the calculations which follow, two assumptions ensure that the ranges obtained are the upper bounds to ranges which can be obtained in practice. In the first condition, both the signal and the noise statistics are assumed known and coherent detection is used. In an actual attempt to locate an object, often very little can be assumed about the expected type of signal and noise. If bounds can be placed on the distance and/or the direction to the source, however, some information, which can be used in processing the received signals, is available concerning the signal's amplitude, frequency spectrum, etc. The greater the *a priori* knowledge of the expected signal, the closer the ranges obtained in an actual search will approximate those given in this article. The second factor, which probably establishes the ranges as the upper bounds, is the neglect of any increase in ambient noise due to the detection process. Possible noise, caused by equipment aboard the submersible, turbulence created by the platform, electrolytic action, etc., has not been considered. Only the noise processes over which the searcher has no control have been included in the present calculations.

Certain parameters pertaining to the ocean environment and to the method of search have been assigned numerical values which will be listed in this article. The dependence of the detection range on some of these parameters is given in Chart 1, Section I. Both the source and detector are assumed near the bottom in 4 km of water; this depth is almost the

average depth of the oceans (ref. 3). The static magnetic field, B_0, has been assigned a value of 40,000 gammas, and the seawater conductivity, σ, is 4 mhos/m. The bottom current and the velocity of the detector are 0.1 knot and 1.0 knot, respectively. The permeability of the ocean and the seabed have been assigned the value of the permeability of free space, $\mu = \mu_0 = 4\pi \times 10^{-7}$ N/A^2. The rationalized mks system is used throughout this article.

BASIC APPROACH

The search scheme used is shown in figure 1.

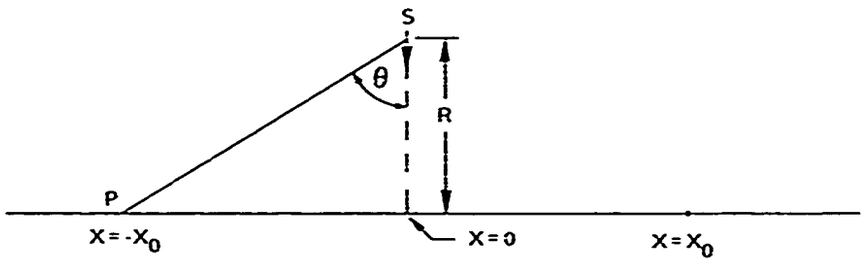

Figure 1. Search scheme.

The platform, P, carrying the detector is assumed to move along a straight horizontal line with the detector at the same depth as the source, S. The platform is assumed to start at some point, $-X_0$, along this line. It then proceeds with the detector past the point of closest approach of the search path with the source and on to $X = +X_0$. At this point, a decision is made concerning the presence or absence of the source. The orientation of the source's dipole moment is assumed horizontal and perpendicular to the platform's path. The angle between the dipole moment of the source and the line drawn from the source to the detector is θ. The distance along the platform's path measured from the point of closest approach, $X = 0$, is then given by $X = R \tan \theta$. In the following discussion, we will be concerned with the spatial variation of signals and the spatial spectral density of noise, although one can also consider their time variation, as seen by the detector, with equivalent results. The connection between the time and the spatial variation is made through the relation, $X = VT - X_0$, where V is the platform's velocity and T is the time.

The detector is assumed to be a single component (scalar) detector, such as a flux-gate magnetometer or electric dipole. It is assumed that this detector is always oriented so that the signal lies along its sensitive direction. This is consistent with our assumption of a coherent search. We will also assume that the noise is independent of the antenna's orientation.

The field due to an infinitesimal dipole in the infinite ocean is

$$\vec{F} = \frac{D}{(X^2 + R^2)^{3/2}} [2 \cos\theta \hat{r} + \sin\theta \hat{\theta}]. \qquad (1)$$

where $D = p/4\pi\sigma$ when $\vec{F} = \vec{E}$, the electric field, and $D = \mu_0 M/4\pi$ when $\vec{F} = \vec{B}$, the magnetic field (refs. 4 and 5). The current and magnetic dipole moments of the sources are p and M.

respectively. The unit vector, $\hat{r}$, is directed from the source to the detector, and $\hat{\theta}$ is a unit vector pointing in the direction of increasing θ. The use of Eq. 1 is justified for the sources considered, providing we are far from the source compared with its dimensions. Because both the source and detector are near the bottom, the electric field for a constant dipole moment can rise to a value twice that given by Eq. 1 (ref. 5). In view of the porosity of the seabed and the inherent uncertainties in the ambient noise, Eq. 1 will be used. For the magnetic dipole, Eq. 1 is correct provided that the permeability of the ocean and the seabed are equal (as assumed) and that the coil is sufficiently insulated so that its electric field is negligible outside the coil.

At the end of the tow, at point X_0, a decision is made concerning the presence or absence of the source. This decision is effected by passing the output of the detector through the appropriate linear filter, which is matched to the signal and ambient noise. This "matched filter" technique will maximize the filter's output signal-to-noise ratio at point X_0 (refs. 6 and 7). The output at point X_0 is then compared with a fixed decision level, related to the detection and false alarm probabilities, and the presence or absence of the source's signal is decided.

For an infinite measuring time, the relationship between the signal, noise, and signal-to-noise ratio (ref. 8) is given by

$$d^2 = \int_{-\infty}^{\infty} \frac{|S(\omega)|^2}{\Phi(\omega)} \frac{d\omega}{2\pi} , \tag{2}$$

where d is the signal-to-noise ratio, ω is the time radian frequency, $S(\omega)$ is the time Fourier transform of the signal, and $\Phi(\omega)$ is the time noise spectral power density. Using the relationships $\omega = VK$, $|S(\omega)|^2 = [|S(K)|^2][|V|^2]$, and $\Phi(K) = V\Phi(\omega)$, Eq. 2 becomes

$$d^2 = \int_{-\infty}^{\infty} \frac{|S(K)|^2}{\Phi(K)} \frac{dK}{2\pi} , \tag{3}$$

where K is the spatial angular frequency, V is the detector's velocity, S(K) is the spatial Fourier transform of the magnitude of Eq. 1, and $\Phi(K)$ is the spatial noise spectral power density. It is interesting to note that the form of Eqs 2 and 3 is indifferent as to whether we measure in the time or spatial domain; however, we will continue to use the spatial viewpoint because we are dealing with static sources. Two assumptions implicit in Eqs. 2 and 3 should be mentioned. Both Eqs. 2 and 3 refer to infinite tow paths; however, because of the rapid decay of Eq. 1 for large X, Eqs. 2 and 3 apply providing we take $|X_0| \geq 3R$. Also, both Eqs. 2 and 3 are applicable only to noise which is stationary and gaussian.

Taking the Fourier transform of Eq. 1, we find that $|S(K)|^2$ is almost constant for $|K| < 1/R$ and decreases rapidly for $|K| > 1/R$. In view of this property, we take $|S(K)|^2$ to be constant for $|K| < 1/R$ and zero otherwise. With this simplification and the use of Parseval's theorem, we obtain

$$d^2 = \int_{-\infty}^{\infty} |\vec{F}|^2 \, dx \left[\frac{\int_0^{f_u} \frac{1}{\Phi(K)} \, df}{f_u} \right] . \tag{4}$$

where f_u is the effective upper cut-off frequency:

$$f_u = \frac{K_u}{2\pi} = \frac{1}{2\pi R} .$$

The left-hand integral in Eq. 4 has the value

$$\int_{-\infty}^{\infty} |\vec{F}|^2 \, dx = D^2 \frac{1}{r^5} (2\pi)^6 \left(\frac{21}{32}\right). \tag{5A}$$

where $r = 2\pi R$ and the term in the bracket in Eq. 4 is the average of the reciprocal of the noise density over the spectrum of the signal, i.e., $0 < f < 1/2\pi R$.

Both the magnetic and electric noise were fit to a noise power density of the form

$$\Phi e, m\,(K) = \frac{Be, m}{K} + Ce, m, \tag{5B}$$

where e refers to the electric noise, m refers to the magnetic noise, and Be,m and Ce,m are a set of four constants. For this noise spectrum, the bracketed term in Eq. 4 is

$$\frac{1}{C}\left[1 - \frac{Br}{2\pi C} \ln\left(1 + \frac{2\pi C}{rB}\right)\right]. \tag{6}$$

Eqs. 5 and 6 can be combined to give

$$r^5 = \frac{G}{d^2}\left[1 - \frac{Br}{2\pi C} \ln\left(1 + \frac{2\pi C}{rB}\right)\right]. \tag{7}$$

where $G = D^2/C\,(2\pi)^6\,(21/32)$.

The value chosen for d, the signal-to-noise ratio, will determine the false alarm probability and the detection probability for a given run. In the present calculations, a value of two is used. This value corresponds to a detection probability of 0.9 and a false alarm probability of 0.2 (ref 8). For the same value of d, one can obtain a greater probability of detection at the expense of a greater false alarm probability and vice versa. Greater values of d will enhance the probability of detection or lessen the false alarm probability when the other is constant. The dependence of the detection range on d is given in Chart 1, Section I.

Before using Eq. 7 to calculate numerical results for the electric and magnetic cases, we will derive its asymptotic forms. For $r \ll (2\pi C)/B$, $(Br)/(2\pi C) \ll 1$ and

$$r = \left(\frac{G}{d^2}\right)^{1/5} . \tag{8}$$

For $r \gg (2\pi C)/B$, $(rB)/(2\pi C) \gg 1$ and

$$r = \left(\frac{2\pi CG}{2Bd^2}\right)^{1/6} \quad (9)$$

Thus, r varies as the one-fifth power of G for small r and as the one-sixth power of G for large r, where r is to be compared with $r_0 = (2\pi C)/B$.

MAGNETIC FIELDS

The first type of magnetic source to be considered is a copper torus through which current is passed. The coil is assumed sufficiently insulated to ensure that there is essentially no current outside the windings. The magnetic moment, M, of such a coil is given by

$$M = \left(\frac{AP\pi r_1^3}{\rho 2}\right)^{1/2} \quad (10)$$

where A is the cross-sectional area (through the windings), P is the power input, r_1 is the large radius of the torus, and ρ is the resistivity of the windings. Using values of $A = \pi(0.1\ m)^2 = 3.14 \times 10^{-2}\ m^2$, P = 10 W, r_1 = 1 m, and $\rho = 1.7 \times 10^{-8}\Omega$-m (i.e., the resistivity of copper), one obtains a magnetic moment of 5.44×10^3 A-m^2. The magnetic moment for different types of coils and input power can be calculated from Eq. 10. It is interesting to note that larger magnetic moments for a fixed coil displacement are possible by increasing the coil's diameter at the expense of its cross-sectional area. For the parameters chosen, the coil's weight is about 2 tons and displaces 0.2 m^3. For a 30-day operating life, this coil will require 170 lb of silver-zinc batteries which displace about 2 ft^3.

The second type of source to be considered is the permanent magnet. This source has the advantage of not requiring any power, but the disadvantage of not having its magnetization readily controllable once it is in the water. Using Alnico 5, we can obtain a permanent magnet with a remnant magnetic induction of 13,100 G (ref. 9), which corresponds to a magnetization of 1.05×10^6 A/m. Again assuming a magnet weight of 2 tons, we obtain a volume of 0.25 m^3, yielding a net dipole moment of 2.61×10^5A-m^2 for this source.

A third type of source is a solenoid that is filled with a high permeability material. The magnetic-field intensity in a solenoid, which is long compared with its diameter, can be written as $H = [1/(2\pi r_3 L)](PW/\rho\rho_w)^{1/2}$, where r_3 is the solenoid's radius, L is its length, W is the weight of the windings, and ρ and ρ_w are the winding's resistivity and weight density, respectively. This formula is strictly true only as the length-to-diameter ratio approaches infinity; however, because of the large value of the ratio in the present case, it is an excellent approximation. Choosing values of r_3 = 0.1 m, L = 2π m, P = 70W, and W = 2 tons, the resulting field intensity for copper ($\rho_w = 8.96 \times 10^3$kg/m^3, $\rho = 1.7 \times 10^{-8}\Omega$-m) is ~93 Oe. Filling the solenoid with a high permeability material will lower the magnetic-field intensity from the value previously given due to the opposing magnetization field. For this geometry, the demagnetization factor, $N/4\pi$, is 4.31×10^{-3} (ref. 9). Assuming the solenoid to be filled with Supermendur, a net magnetic-field intensity of 10 Oe is obtained from its magnetization curve (ref. 9) and the demagnetization factor. At this field strength, the magnetic induction is 20,000 G, and the magnetization is 1.6×10^6 A/m, which is near saturation. The permeable core has a volume of ~0.2 m^3 so that the total magnetic dipole moment is 3.2×10^5 A-m^2. In addition to the 2-ton weight of the copper, the Supermendur weighs about 1.8 tons and the

battery weight for 1 month of operation is about 0.6 ton. It is interesting to note that the copper coil previously considered, when run at a power level of 70 W, will yield a dipole moment of 1.4×10^4 A/m, a factor approximately 20 times lower than that for the filled solenoid.

The last source to be considered is a superconducting coil. Recent proposals have indicated the feasibility of constructing large superconducting coils with magnetic moments of approximately 10^7 A-m^2. For a superconducting coil of 1-m radius, a magnetic moment of 3.56×10^6 A-m^2 appears feasible using a matrix of type II superconductor and normal metal. Because the critical field for the best superconductors is about one order of magnitude higher than that for the saturation induction of the highest permeability materials, the order-of-magnitude increase in the dipole moment upon moving from the filled solenoid to the superconducting coil is reasonable.

Natural magnetic noise arises from such temporal sources as solar activity, ionospheric activity, and the motion of seawater through e earth's magnetic field. Except for occasional disturbed periods and the diurnal variations, these noise sources are associated with daily excursions of approximately a few gammas [$1\gamma = 10^{-5}$ G]. In a search for static magnetic fields, Spiess, Mudie, and Lowenstien (SML) (ref. 10) have shown that the major environmental limitation comes from short wavelength anomalies superimposed on the earth's dipole field. Their results will be used to estimate the magnetic noise that might be encountered on a search as proposed in this article. Due to the necessity of interpolating data from SML's graphs, an error in our noise figures of a factor of two should be allowed. Because the range varies as the fifth power of the reciprocal of the average noise, this error, however, represents only a small error in the estimated range.

Based on Eq. 5B, two relationships will be needed to specify the noise power density. Thus, an expanded scale version of SML's magnetometer trace was obtained and a 10-km portion was digitized and Fourier analyzed. It was noted that the resulting spectrum increased rapidly for spatial frequencies less than 0.001 cpm. Because Φ in Eq. 5B increases rapidly for $f < B/(2\pi C)$, $B/(2\pi C)$ was set equal to 0.001 Hz. A second relationship was obtained by relating the variance of the filtered spectrum given by SML to the integral of the noise power spectrum across their bandpass. The rms value of the filtered noise, obtained from the SML spectrum, was halved in an attempt to include the fact that their spectrum was taken in an area of "high magnetic roughness." The resulting rms noise was then reduced by another factor of $1/\sqrt{3}$ to account for the reduction in noise, assuming isotropy, that would be obtained by replacing the SML total field magnetometer with the one-component magnetometer assumed in this article. This final adjusted value of rms noise was compared with the integral of Φ across the SML bandpass to yield the second condition on B and C. The resulting values are $B = 49.62\gamma^2$ and $C = 7.897 \times 10^3\ \gamma^2$-m. These values plus the values for the magnetization and the formulas previously given are sufficient to estimate the maximum range in a magnetic search.

ELECTRIC FIELDS

For the present calculation, the source of the electric field is considered to be an insulated linear conductor terminated in conducting spheres. It is assumed that the diameter of the conductor-insulator combination is small when compared with the diameter of the sphere and that the IR drop along the wire is negligible when compared with the applied EMF. The EMF is assumed to be inserted along a length of the antenna and to have an internal resistance that is small compared with the antenna's.

Because of the remarks made in the section, *Basic Approach*, the input resistance will be that of the antenna in infinite space. Because of the assumption made concerning the antenna wire, the input resistance will be the resistance between the two terminating spheres in the absence of wire. For this case, we can use the resistance capacitance analogy which relates the resistance, R, between the spheres in an infinite medium of conductivity, σ, to their capacitance, C', *in vacuo* through the relationship $R = \epsilon_0/\sigma C'$ (ref. 11). The capacity between two spheres of radius r_s with their centers a distance d apart is given by

$$C' = 2\pi\epsilon_0 r_s \sinh\beta \sum_{n=1}^{\infty} [\operatorname{csch}(2n-1)\beta + \operatorname{csch} 2n\beta],$$

where $\cosh\beta = d/2r_s$ (ref. 12). Choosing $d = 2\pi$ m and $r_s = 0.1$ m, we have $d \gg r_s$ for which $C' = 2\pi\epsilon_0 r_s$. The resistance is then given by

$$R = \frac{1}{2\pi r_s \sigma}.$$

From Eqs. 5 and 7,

$$G = \frac{1}{C}\left(\frac{p}{4\pi\sigma}\right)^2 (2\pi)^6 \left(\frac{21}{32}\right).$$

where $p = Id = (P/R)^{1/2}$ (d is the dipole moment). Using values of $r_s = 0.1$ m and $d = 2\pi$ m, we find that

$$G = \frac{1.585 \times 10^3 \, |P| V^2\text{-}m^4}{C}.$$

where $|P|$ is the power expressed in watts.

Natural electric noise arises from three sources. The first source corresponds to temporal fluctuations arising outside of the earth and propagating beneath the ocean's surface. Using noise figures given by Liebermann (ref. 13) and Cox *et al* (ref. 14) and assuming an infinitely deep sea, we find the electric noise ranges from 1.0 to 4.0 x 10^{-15} $(V/m)^2/Hz$ for frequencies between 0.003 to 0.001 Hz. Viewed as a spatial variation, this corresponds to a noise power density of 0.51 to 2.6 x 10^{-15} $(V/m)^2/cpm$ for frequencies between 0.002 and 0.006 cpm for a detector speed of 1 knot.

The interaction between the movement of the water and the ambient magnetic field will also cause an electric field. The magnitude of this field depends to some extent upon the ability of the surrounding water to "short circuit" the potential across the water in the vicinity of the receiving antenna. For the completely short-circuited case, the electric field along the antenna is given by the product of V_H and B_V, where V_H is the component of velocity perpendicular to the antenna and B_V is the vertical magnetic field (ref. 15). If we divide both B_V and V_H into their (spatially) constant and varying components, the resulting product will contain four terms. One of these terms will be constant and can be neglected because it will be rejected by our matched filter. A second term, relating the two spatially varying parts, will be small. The remaining two terms represent the interaction of the constant part of the velocity with the varying part of the magnetic field and vice versa. The former term is the product of the square of the mean velocity and the magnetic-noise power spectrum.

which was calculated earlier. At a frequency of 0.001 cpm, this is 4×10^{-15} $(V/m)^2$/cpm.

Both these sources are dominated by velocity fluctuations interacting with the earth's field. The velocity fluctuations used in this article were measured 0.75 to 1.75 m off the bottom in water 12 to 20 m deep in an area off Red Wharf Bay (~53°20'N – 4°10'W). Whether the form of the turbulence spectrum is maintained in deeper water has not been determined. Four points of the low-frequency end of the Red Wharf Bay data were fit to a straight line of the form $\Phi(\omega) = A'/f_w + B'$, where $\Phi(\omega)$ is the turbulent noise power measured on the bottom, f_w is the time frequency, and A' and B' are constants depending on the mean current. To obtain the needed values, it was necessary to extrapolate the observed data by a factor of 10; however, the straight line fit had a correlation coefficient of 0.97. The velocity noise spectrum, viewed as carried along with the mean current, was then found to be $\Phi(K) = (0.102U)^2 (7.93Usec + 0.04656/f_s)$, where U is the rms current and f_s is the spatial frequency. The electric noise power density will be B_v^2 times this value. Inserting values of U = 0.1 knot and B_v = 40,000 gammas and comparing the result with Eq. 5B, we obtain $B = 1.3 \times 10^{-14}$ $(V/m)^2$ and $C = 1.8 \times 10^{-14}$ m $(V/m)^2$ for the electric-noise coefficients. These coefficients, plus the expression for the electric signal, allow us to calculate range as a function of input power by the method outlined in the section, *Basic Approach*.

It should be noted that electric "velocity" noise dominates "atmospheric" noise only if the mean current exceeds a certain minimum. For the values of noise in this article, this minimum current is 0.1 cm/sec. The present analysis does not extend to currents lower than this value.

RESULTS AND DISCUSSION

Figure 2 shows the variation of range with increasing magnetic moment. It is interesting to note that increasing the source's magnetic moment by a factor of 10^5 increases the maximum range by less than a factor of 10. Near a magnetization $M = 1 \times 10^2$ A-m^2, the range increases as $R \sim M^{0.390}$, while for M near 1×10^7 A-m^2, $R \sim M^{0.348}$. Over the entire range, 1×10^2 A-m^2 < M < 1×10^7 A-m^2, $R \sim M^{0.370}$. The variation of the slope with magnetization is indicative of the competition between the "white" and 1/f portions of the noise spectrum. Knowing the variation of R with M and the dependence of M on various parameters, the variation of R with these parameters can be determined. This dependence is listed in Chart 1, Section I. The variation of R with these parameters is unexceptional except for the large increase in range with the diameter of the copper coil as compared with an increase in its input power.

The range of an electric dipole as a function of input power is given in figure 3. The range obeys a $P^{1/6}$ dependence on the power at all power levels between 10^{-1} and 10^4 W. This behavior is due to the dominance of 1/f-type noise.

It is interesting to note the strength of the signal at the distance of closest approach for the magnetic and electric cases. At this point, the magnetic field has a value of 74 gammas for a dipole strength of 100 A-m^2 and a value of 22 gammas for a dipole strength of 10^7 A-m^2. These values are well within the sensitivity of conventional magnetometers, and sensitivities of this type have been exhibited in the ocean environment. For the electric field, the potential across the ends of an antenna of length 2π m will be about 2 μV. This level can be measured by standard potentiometer techniques; however, care must be exercised to minimize thermal EMF's, turbulence introduced into the water by the detector or platform, and electrolytic action on the receiving electrodes.

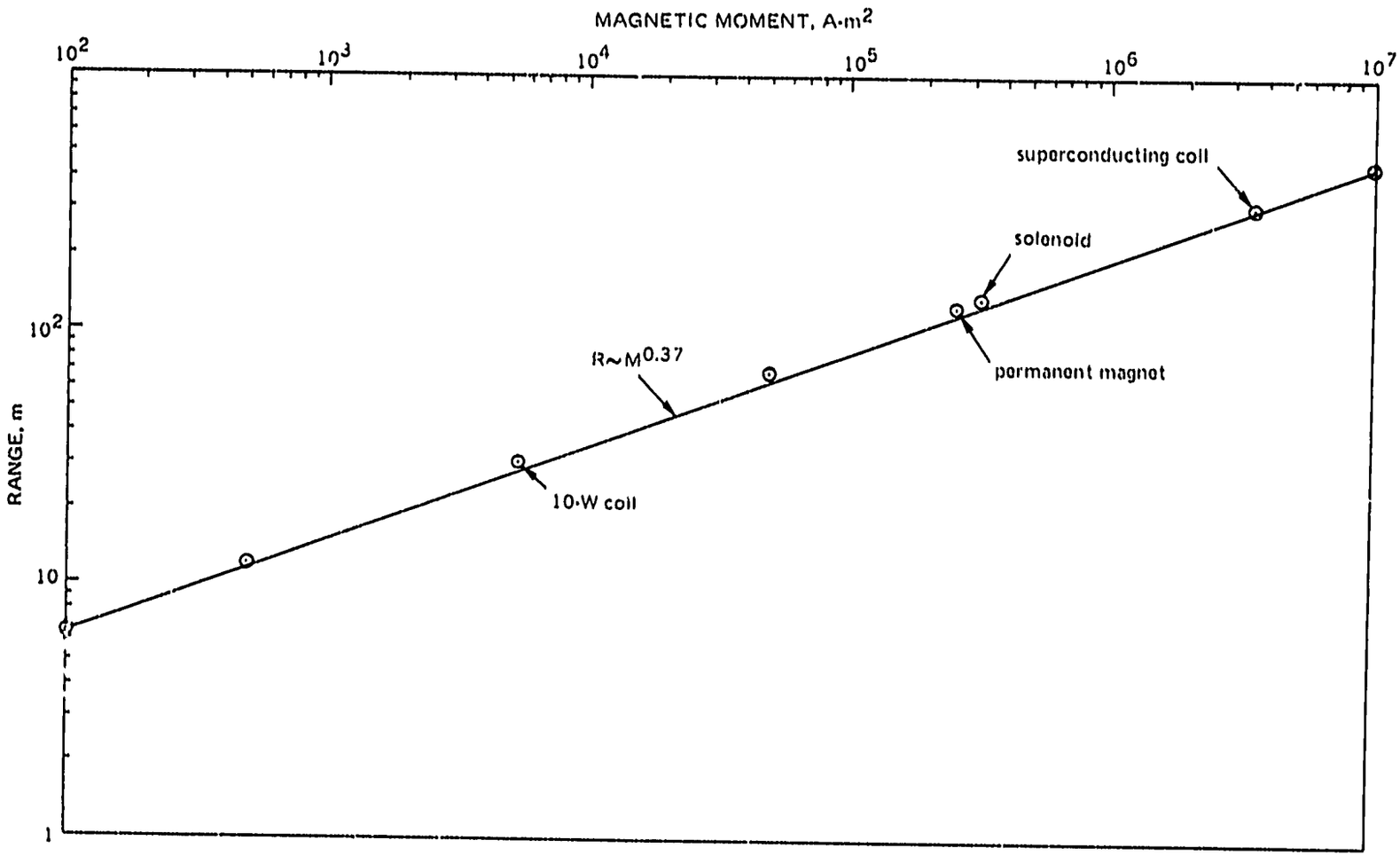

Figure 2. Range variation caused by increasing magnetic moment.

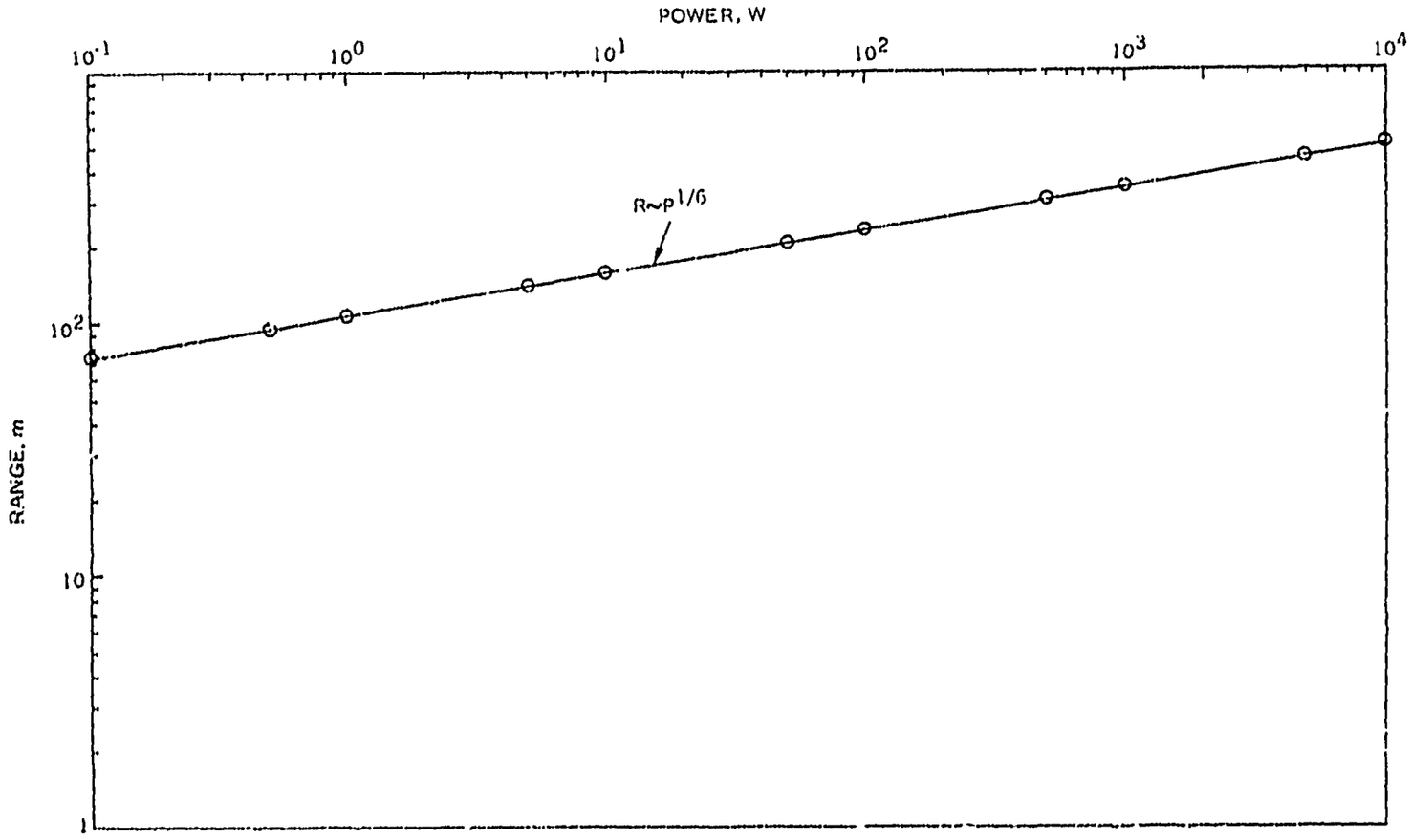

Figure 3. Range of electric dipole as a function of input power.

The question still remains as to whether the ranges predicted in this article are typical of the oceanic environment as a whole: Range will change in different geographical locations due to variations in the effective noise power density. If it is assumed that the form of this function changes very little from the form in this article, the noise spectrum will be proportional to the variance of the noise across the passband. For the magnetic case, it is estimated that on a worldwide basis the rms noise can vary by a factor of six: this implies that the obtainable range can vary by a factor of about two. For the electrical case, deep ocean currents can assume values of approximately 0.01 to 0.5 knot (ref. 16). These values imply ranges varying from a factor 2.3 times greater to a factor 1.8 times smaller than those in this article. The large variability of the maximum range obtained thus emphasizes the dependence of search effectiveness on environmental parameters.

REFERENCES

1. C. Fitzhugh Grice. Finding Underwater Objects. *Ocean Industry*. v. 3, no. 1, pp. 25–42. 1968, and v. 3, no. 2, pp. 28–39, 1968.

2. F. N. Spiess and A. E. Maxwell. Search for the Thresher. *Science*. v. 145, pp. 349–355, 1964.

3. A. C. Vine. Physical Oceanography in *Handbook of Ocean and Underwater Engineering*. pp. 1–4. McGraw-Hill Book Company, New York, 1969.

4. E. U. Condon. Static and Magnetic Fields in *Handbook of Physics*. pp. 4–24. McGraw-Hill Book Company, New York, 1958.

5. A. Baños, Jr. and J. P. Wesley. *The Horizontal Electric Dipole in a Conducting Half Space*. p. 83. Scripps Institute of Oceanography. Report No. 53-33, September 1953.

6. B. M. Dwork. The Detection of a Pulse Superimposed on Fluctuation Noise. *Proc. I.R.E.* v. 38, pp.771–774, July 1960.

7. G. L. Turin. An Introduction to Matched Filters. *Trans. I.R.E.* v. IT-6, pp. 311–329, June 1960.

8. C. W. Helstrom. *Statistical Theory of Signal Detection*. pp. 121 and 107. Pergamon Press, New York, 1968.

9. R. M. Bozorth, T. R. McGuire, and R. P. Hudson. Magnetic Properties of Materials in *American Institute of Physics Handbook, 2nd Edition*. pp. 5-188, 5-233, and 5-177. McGraw-Hill Book Company, New York, 1963.

10. F. N. Spiess, J. D. Mudie, and C. Lowenstein. Environmental Limitations to Deep Sea Search. *Proc. 4th U. S. Navy Symposium on Military Oceanography*. pp. 69–80. Naval Research Laboratory, 1967.

11. W. T. Scott. *The Physics of Electricity and Magnetism, 2nd Edition.* p. 197. John Wiley & Sons, Inc., New York, 1966.

12. W. R. Smythe. Definitions, Units, Nomenclature, Symbols, Conversion Tables in *American Institute of Physics Handbook, 2nd Edition.* pp. 5–14. McGraw-Hill Book Company New York, 1963.

13. L. N. Liebermann. Other Electromagnetic Radiation in *The Sea*. M. N. Hill, ed. v. I. p. 474. Interscience Publishers, New York, 1962.

14. C. Cox, T. Teramoto, J. Filloux. On Coherent Electric and Magnetic Fluctuations in the Sea in *Studies on Oceanography*. K. Yoshida, ed. Univ. of Washington Press. 1965.

15. M. S. Longuet-Higgins, M. E. Stern, H. Stommel. The Electrical Field Induced by Ocean Currents and Waves, With Applications to the Method of Towed Electrodes. *Papers in Physical Oceanography and Meteorology* v. 13, no. 1, 1954.

16. A. C. Vine. Currents and Circulation in *Handbook of Ocean and Underwater Engineering*. pp. 1–72. McGraw-Hill Book Company, New York. 1969.

DETECTION OF RADIOACTIVE BEACONS IN THE OCEAN

by

E. J. Wesley
NUC

CONTENTS

DETECTION OF RADIOACTIVE BEACONS IN THE OCEAN

Two approaches to the detection of radioactive beacons in water are discussed in this article: detection of a point source of radioactivity on the bottom or in open water and detection of induced activity from a neutron source in open water.

DETECTION OF A RADIOACTIVE POINT SOURCE UNDERWATER

The range of nuclear radiation in water is quite limited. This is true whether considering alpha, beta, or gamma rays, or neutrons, all of which are readily attenuated by water. For gamma rays, the intensity from a point source can be calculated from the following relationship:

$$I = N_0 \frac{\bar{B}e^{-\mu R}}{4\pi R^2} ,$$

where R is the range from the source; μ is the linear attenuation coefficient (for energy); $\bar{B}$ is a buildup factor to account for photons that have been scattered and lost energy, but have not been lost to the beam; N_0 is the original intensity; and I is the photon density at R. At very short ranges ($\mu R \ll 1$), the inverse square term, $1/(4\pi R^2)$, controls the change in photon density as a function of distance. At three mean-free-paths (the distance $R_0 = 1/\mu$), the inverse square and attenuation are equally effective; beyond three R_0, the attenuation term becomes progressively more dominant. In air, R_0 is approximately hundreds of feet (419 ft at 1.0 MeV) (ref. 1), but underwater R_0 is very short (14 cm at 1 MeV and a maximum of 60 cm for energies greater than 25 MeV). For a 100-Ci point source of ^{60}Co, the detection range underwater is approximately 9 ft (I is equal to the gamma-ray background of seawater). Even with a high-energy machine (25 MeV), the range for a yield equivalent to 100 Ci will be no more than 28 ft. At best, gamma-ray sources are short-range beacons.

Neutron sources are equally short range when considering detection of the source neutron. For fast neutrons from a fission source, i.e., ^{252}Cf, the flux density decreases by a factor of 10 every 10 cm (at a 1-ft range) to 20 cm (at a 3-ft increase in range). Neutrons from a 10^{11} n/sec source (a large source by present standards) will hardly be detectable beyond 8 ft.

Among the nuclear particles, only neutrinos penetrate water readily. Their low interaction rate with matter makes detection extremely inefficient and establishes a very high background flux, primarily from extraterrestial sources. Both facets, the lack of a suitable detecter and the probable high background, negate consideration of a neutrino beacon.

DETECTION OF NEUTRON-INDUCED ACTIVITY IN SEAWATER

Most neutrons from a point source in water are thermalized and captured within approximately 1 ft of the source. In the process, a series of radioactive isotopes is induced in the seawater surrounding the source. Most prominent among the gamma-ray emitters

induced by this process are ^{38}Cl (38 min) and ^{24}Na (15 hr). If the seawater surrounding the source flows past the source, the induced activity will be carried from the source in the same manner that smoke is carried by air from a campfire. The induced activity can be detected, at a considerable range from a point source, as a distributed source of active water. For a neutron source of 10^{11} n/sec in a current of 1 knot, the induced activity in seawater passing within 1 ft of the source, is approximately 6×10^{-9} Ci/l. This is 2×10^{2} times the natural background of seawater. Assume that the cross sectional area of this stream of active solution, which is approximately 0.28 m^2, gradually increases as it is carried away by the current. The activity, 1 hr later, will be 1 km downstream with a frontal area of 500 m^2, a nominal diffusion growth (ref. 2); however, it will still be readily and unambiguously detected with present underwater detection systems. If the currents are negligible and if the activity drifts around so that the general region becomes activated (i.e., smokey), 10^{11} n/sec will induce enough activity to double the background in 8×10^{5} m^3 of seawater. In practical situations, the activity will not be uniformly distributed and the "smoke" will constitute a trail to be followed to the source. In the final approach to a neutron source in seawater, the captured gamma rays, which are emitted each time a neutron is captured, will clearly define the area (ref. 3). These captured rays from seawater are high-energy gamma rays that can probably be detected at 16-ft ranges from a 10^{11}-n/sec source.

The problem of hazard, primarily to the environment, is nonexistent a few feet from a gamma emitter; however, the problem should still be considered when neutron sources are used to induce activity in seawater. This problem can be discussed in terms of the AEC requirement for disposal of radioisotopes into sewers. For ^{24}Na and ^{38}Cl, the maximum permissible concentration in water for continuous exposure to the population at large is 3×10^{-7} Ci l (ref. 4). This is 50 times the concentration calculated for the initial activation of seawater flowing at 1 knot past a 10^{11}-n/sec source. If the flow is so slight that the activity is essentially distributed by diffusion, the concentration of ^{24}Na becomes the principal hazard. At equilibrium, where the decay rate equals the rate of formation, the total ^{24}Na activity in seawater from a 10^{11}-n/sec source is 0.03 Ci. If this is distributed or averaged over a volume of $10^{2}m^{3}$* or more, this concentration will be equal to or below the AEC maximum permissible concentration. The equilibrium period for ^{24}Na is 21.6 hr; thus, if the flow is such that the water is exchanged within 14 ft of the source at least once in 21.6 hr, the volume of water with a concentration above the AEC limit will be even smaller. Diffusion rates near the bottom generally exceed this flow rate (ref. 2), and it is unlikely that a neutron source implanted in the ocean will ever constitute a hazard to the environment beyond a few feet of the source.

BEACON SYSTEM

A radioactive beacon system consists of a source implanted above the bottom and a detector aboard the search vessel. The source, a radioisotope in a corrosion-resistant housing, will not require auxiliary power, and it can be selected to last "indefinitely" compared with probable periods of use. When a bare source is handled in the water, immediate contact must be avoided, and it is probable that a small shield will be necessary to facilitate implantment and removal. Some form of shield must be provided on the surface to protect personnel during transport of relatively large sources. While the implantment of sources in the bottom is possible, the background radioactivity of the bottom is generally 10 to 1000 times that of open seawater, and the detection range (above background) will be shortened several feet.

*This is equal to a cube approximately 14 ft per side.

In most instances, it is desirable to locate the source 6 ft or more above the bottom. This is particularly true when the flow of seawater containing activation products is used to extend the detection range.

The receivers for a beacon system will be scintillation detectors. Underwater systems using NaI detectors, which measure either 4 in. in diameter x 4-in. thick or 2 in. in diameter x 8-in. long, have been successfully used to measure the natural activity levels in seawater. The small diameter systems are extremely rugged and have been assembled in arrays capable of detecting activity changes of 2 to 5 percent of the ^{40}K background. A level of 10 percent of the ^{40}K activity was used in the previous range calculations (this can be obtained with a single detector).

The cost of a beacon system using gamma-ray emitters would be nominal, less than $5K for the source and $20K for a detector-ratemeter system (assuming the R&D costs can be spread across several systems). Pricing of high-intensity neutron systems is uncertain. A projected price for ^{252}Cf in 1980 is $25K for 10^{11} n/sec (AEC) or approximately 20 mg. This amounted to the world supply a few years ago. Availability is dependent on a pending AEC decision to produce ^{252}Cf in relatively large quantities. No other neutron sources appear satisfactory for this application.

REFERENCES

1. S. Kinsman. *Radiological Health Handbook.* U. S. Department of Health, Education, and Welfare, Public Health Service, October 1955.

2. A. Okubo and D. W. Pritchard. *Summary of Our Present Knowledge of the Physical Processes of Mixing in the Ocean and Coastal Waters, and a Set of Practical Guidelines for the Application of Existing Diffusion Equations in the Preparation of Nuclear Safety Evaluations of the Use of Nuclear Power Sources in the Sea.* Chesapeake Bay Institute, The Johns Hopkin University, NYO-3109-40, Reference 69-1, September 1969 (AEC Contract No. AT(30-1)-3109).

3. R. C. Greenwood and J. H. Reed. *Prompt Gamma Rays from Radiative Capture of Thermal Neutrons.* IITRI-1193-53, October 1965.

4. *Maximum Permissible Body Burdens and Maximum Permissible Concentrations of Radionuclides in Air and in Water for Occupational Exposure.* U. S. Department of Commerce, National Bureau of Standards Handbook 69, June 1959.

CHEMICAL SYSTEMS AS POTENTIAL UNDERSEA NAVIGATIONAL AIDS

by

S. Yamamoto
W. H. Shipman
A. R. Zirino
NUC

CONTENTS

CHEMICAL SYSTEMS AS POTENTIAL UNDERSEA NAVIGATIONAL AIDS

INTRODUCTION

This article summarizes a variety of chemical methods which might serve as potential undersea navigation aids. In this survey, two general categories will be considered: mapping of the natural chemical environment and introduction of chemical markers into the ocean-bottom environment. This discussion will be limited to those chemical parameters which can be measured *in situ* by remote probes or samplers. These parameters and the background levels for average ocean water are in table 1. It should be noted that this table lists only those parameters for which direct *in situ* measurement systems are currently available; development of new *in situ* measurement techniques would expand this list. In addition, the number of potential methods would be increased if laboratory-type measurements were included because such methods are more plentiful and are generally more sensitive and accurate.

MAPPING OF THE NATURAL CHEMICAL ENVIRONMENT

We define chemical mapping as the use of natural variations in a given chemical parameter or variations in the distribution of several chemical parameters as navigational aids. Either the seawater or the bottom sediment can be mapped; the former, however, is probably less reliable due to the dynamic nature of the water mass.

Bottom Seawater

A search of the literature revealed essentially no information regarding horizontal variations in the chemical constituency of deep ocean bottom water over a relatively small area, i.e., several square miles. In fact, there is little information on the vertical distribution of chemicals near the bottom. It is probably reasonable to assume that there will be little or no horizontal variation in either the major chemical constituents or the composite parameters (such as salinity or density); however, there might be marked variations in the concentrations of trace constituents. Unfortunately, this is one region of the ocean for which little is known concerning the chemistry.

Bottom Sediments

There is considerable information in the literature regarding the chemical composition of deep sea sediments. Composition varies with the nature of the sediment, its location, particle size, absorptive properties, etc. Again, however, little is known about variability over a relatively small area of the bottom. Therefore, no statement can presently be made concerning the usefulness of sediment mapping for navigational purposes.

Table 1. Chemical Parameters That Can Be Measured *In Situ*.

Measurement Parameter	Background (Average Ocean Water)	Detector	Detection Limit	Precision	Equipment Cost	Equipment Weight	References
Salinity	30 to 40‰	Temperature-chlorinity-depth recorder	-	±0.05‰	$25,000	200 lb	Ref. 1
		Induction-conductivity-temperature recorder	-	±0.02‰			
Density	1.016 to 1.032 g/ml	Calculated from temperature-salinity data	--	± 0.0001 g/ml	$25,000	200 lb	Ref. 2
Turbidity	Highly variable Function of particulate concentration, size distribution, chemical composition	Colorimeter	Function of particle size, opaqueness, light, wavelengths, chemical composition		$ 2000	50 lb	Ref. 3
Fluorescence	Varies with instrument parameters, e.g., wavelength	Fluorimeter, continuous flow	-	--	$ 2000	50 lb	Ref. 4 Ref. 5
Dissolved O_2	0.1 to 7 ml/l	Electrode	0.01 ml/l	±0.01 ml/l	$ 1500	100 lb	Ref. 6
Eh	-0.2 to +2 V	Electrodes		±0.010 V	$ 1000	50 lb	Ref. 7
pH	7.5 to 8.5	Electrodes		±0.01 pH units	$ 1000	50 lb	Ref. 6
NO_3	1 to 5 ppm	Specific ion electrode	0.6 ppm		$ 1500	50 lb	Ref. 8
Cu^{++}	0.003 ppm	Specific ion electrode	0.6 ppm		$ 1500	50 lb	Ref. 8

Table 1. Continued.

Measurement Parameter	Background (Average Ocean Water)	Detector	Detection Limit	Precision	Equipment Cost	Equipment Weight	References
ClO_4	Unknown, ~ 0	Specific ion electrode	1 ppm	-	$ 1500	50 lb	Ref. 8
CN^-	Unknown	Specific ion electrode	25 ppb	--	$ 1500	50 lb	Ref. 8
F^-	1 ppm	Specific ion electrode	25 ppb	-	$ 1500	50 lb	Ref. 8
$S^=$	0 to 10 ppm	Specific ion electrode	$< 3.2 \times 10^{-10}$ ppb	--	$ 1500	50 lb	Ref. 8
Ag^+	0.04 ppb	Specific ion electrode	10 ppb	--	$ 1500	50 lb	Ref. 8
Br^-	67 ppm	Specific ion electrode	10 ppb		$ 1500	50 lb	Ref. 8
I^-	0.06 ppm	Specific ion electrode	1 ppb	--	$ 1500	50 lb	Ref. 8
Hg^{++}	0.03 ppb	Specific ion electrode	2 ppb	-	$ 1500	50 lb	Ref. 9
Natural radioactivity	350 pCi/l	Gamma-ray detectors	30 pCi/l		$25,000	500 lb	--
Elemental composition	Ref 6, p. 154	X-ray fluorescence analysis	ppm range		$10,000 to $20,000	300 lb	--
		Neutron activation analysis	ppb range		$25,000 +	1000 lb	--

UV SCANS. Because a number of compounds that fluoresce under ultraviolet radiation exist in the sediment, an ultraviolet scan of the bottom might be a useful adjunct to visual observations.

Summary

Mapping of the chemical environment, either of the seawater or of the sediment, does not appear promising. Too little is known about variations in the chemical parameters over a relatively small area of the ocean bottom.

CHEMICAL MARKERS

Any chemical agent that can be introduced into the sea and then be detected can potentially serve as a marker. For the purposes of this discussion, the markers are divided into two categories: soluble and insoluble chemical systems.

Soluble Markers

Soluble markers have the advantage of being more easily detected than insoluble markers, but they are also subject to the vagaries of the transport processes that occur in the ocean environment.

There are three possible ways by which these markers can be introduced: instantaneous release; pulsed release at either fixed time intervals or upon interrogation, and continuous release. Release of soluble markers will generate concentration fields whose features will depend upon parameters which describe the transport processes in the ocean. (These parameters are factors such as currents, eddy diffusion, and shear forces.) Detailed calculations based on an ocean diffusion model of these concentration fields have been made by Mikhail and his associates (refs. 10 and 11). The discussion which follows is based entirely on their results. It should be noted that the model used by Mikhail assumed an infinite ocean environment, thus, it is not strictly applicable to a situation in which material is released at or near the bottom. Mikhail's results, however, are useful for this article because the vertical dimensions of the marker patches are relatively small when compared with the horizontal dimensions. A second point to note is that the discussion is based on calculations made for ocean conditions off Cape Kennedy in August (table 2). The actual conditions in any given zone of the ocean at any given time can, of course, be quite different; however, the results of Mikhail's calculations are representative of at least one set of actual conditions encountered in the ocean.

Table 2. Standard Ocean Conditions, Based on Conditions Existing Off Cape Kennedy in August (Ref. 10).

Condition	Measurement
Eddy diffusivity in X direction	1400 m^2/hr
Eddy diffusivity in Y direction	1400 m^2/hr
Eddy diffusivity in Z direction	0.47 m^2/hr
Horizontal shear	0.0 hr^{-1}
Vertical shear	23.8 hr^{-1}
Mean current velocity	360 m/hr (10 cm/sec)

INSTANTANEOUS RELEASE. When a point source containing a quantity, M_0, of a soluble chemical is instantaneously released into the sea, an ellipsoidal patch is formed that expands with time and drifts downstream with the current. The volume of the patch within which the concentration exceeds the minimum detectable amount, D_0, will increase to a maximum, V_{max}, with time and then decrease to zero. Figure 1 shows changes in the horizontal dimensions of the patch with time; these changes were calculated by Mikhail for standard ocean conditions (table 2) in which the ratio of the amount released to the minimum detectable amount, M_0/D_0, was 2.2×10^9 m^3. The shapes in figure 1 are essentially representative of the overall shapes because the vertical dimensions are very small when compared with the horizontal dimensions. Because the patch drifts along with the current, the center of each patch in the figure will also move with the current and its position will depend upon the magnitude and the direction of the current.

Therefore, although concentration gradients exist within the patch, the instantaneous release method can be used for navigation purposes only if the magnitude and direction of the current are known and if they are uniform over the area of interest during the patch's lifetime.

The patch volume at a given time after release is directly proportional to the ratio, M_0/D_0. The time of the maximum patch volume and the patch's lifetime are also related to M_0/D_0 (but not linearly). Hence, patch size and lifetime will be relatively small if a small amount of material is released and/or if the minimum detectable concentration for the substance is high. These factors are illustrated for Rhodamine B dye in table 3.

Table 3. Instantaneous Release of Rhodamine B Dye; Patch Size and Lifetime as a Function of Amount Released Under Ocean Conditions Listed in Table 2. Minimum Detection Limit, D_0 = 0.01 ppb.

	Case 1	Case 2
M_0/D_0	2.2×10^9	4.4×10^9
M_0	22 kg	44 kg
Patch lifetime	175 hr	231 hr
Time of maximum volume	96 hr	127 hr
Dimensions of maximum volume		
X	21,000 m	33,000 m
Y	900 m	1,030 m
Z	8.3 m	9.5 m

From this brief discussion, it is apparent that an instantaneous release marker would be useful only in situations where a relatively short-lived marker is desired and where the water movement is both known and uniform. The latter requirement can be difficult to fulfill. Bottom currents are complex and vary with topography, depth, surface and middepth current dynamics, tidal forces, and sediment slope stability. They have been found to vary from 0 to 25 cm/sec although they more commonly range from a few tenths to approximately 5 cm sec.*

*W. F. Potter, NUC, private communication.

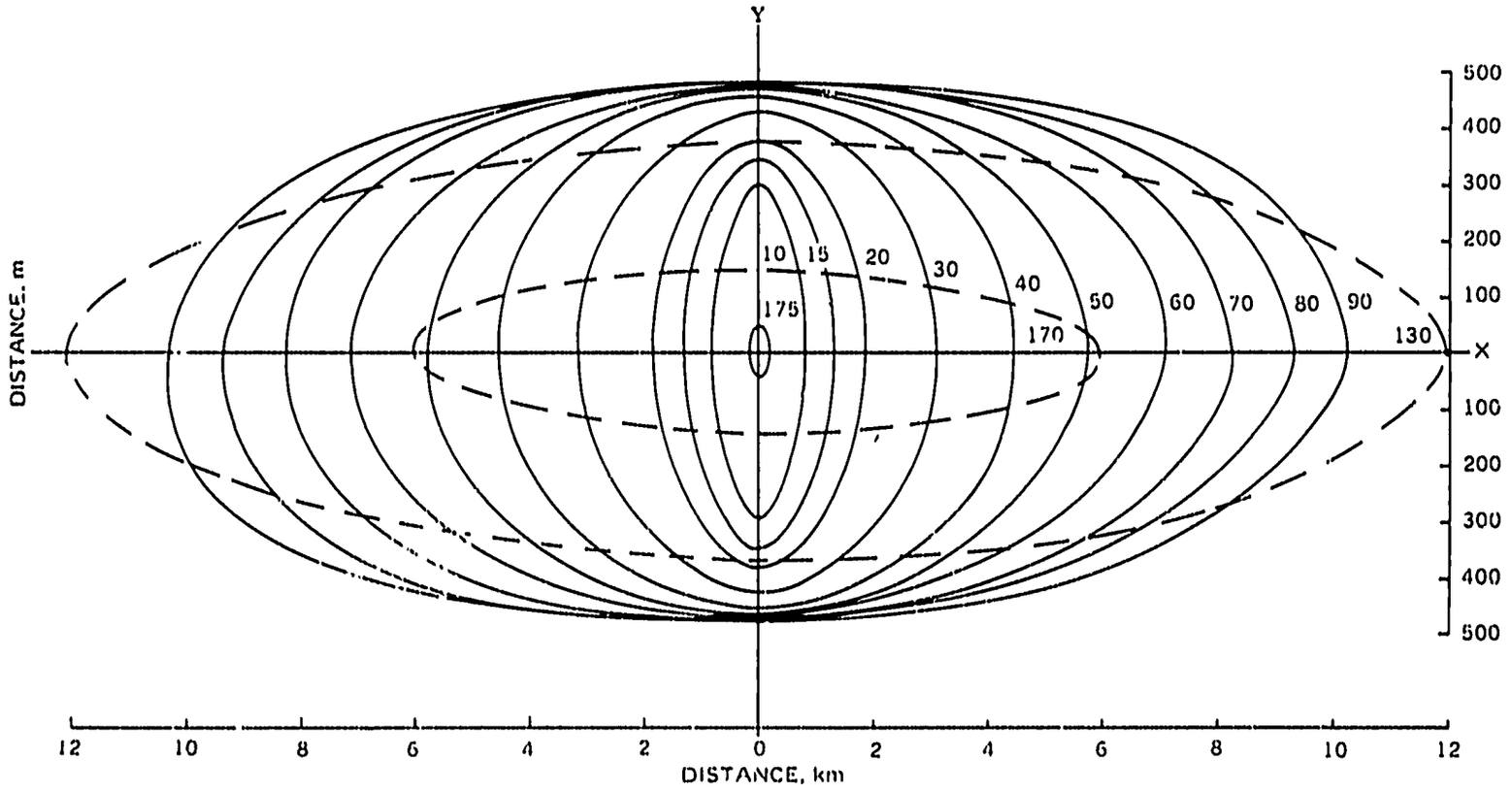

Figure 1. Isoconcentration lines at various times after instantaneous release under the standard ocean conditions listed in table 2. The ellipses represent horizontal cross sections of the patch volume within which the concentration is $\geq$ the minimum detectable concentration, D_0. The ratio M_0/D_0 is 2.2×10^9 m^3.

In addition, the magnitude and direction of bottom currents at a given point vary with time.* Thus, the usefulness of instantaneous release markers appears to be highly limited.

PULSED RELEASE. In this case, there is a series of instantaneous releases. If the time interval between successive releases is long relative to the patch lifetime, there will be a number of independent patches which emanate from the same point and behave as those described in the previous section. If the time interval is short when compared with the patch lifetime, the situation will be similar to that of continuous release. Finally, if the time interval between releases is neither very long nor very short, the situation will be confusing. Thus, this mode of release will be unsuitable for navigation purposes.

CONTINUOUS RELEASE. When a soluble substance is continuously released into the sea, a steady state will be established in which there are concentration gradients. The shapes of the isoconcentration surfaces will depend on the values of the parameters which define the transport process. For a given ocean state, the volume of the patch within which the concentration exceeds the minimum detectable amount is a function of the release rate, R_0, and the detection limit, D_0. For the standard ocean conditions adopted by Mikhail and for a current of 360 m/hr (10 cm/sec), the patch volume, V, is given by

$$V = 1.18 \times 10^6 (R_0/D_0)^{2.05} m^3 .$$

In the following discussion, the ratio R_0/D_0 is 10^6 m^3/hr. For this value of R_0/D_0 at a current speed of 360 m/hr and under standard ocean conditions (table 2), the concentration gradient along the direction of the current at steady state is shown in figure 2. Under these circumstances, the patch extends more than 3 km downstream. The maximum width of the patch is 270 m; the maximum height, 5 m; and the time to achieve steady state, 2.5 hr. This type of patch will, therefore, have a potential range of 3 km and can be used to locate a fixed point on the ocean floor. A current speed of 10 cm/sec is somewhat higher than the speed generally encountered near the bottom at 10,000 to 20,000 ft; currents in these regions range from 5 to 0.5 cm/sec.* Mikhail's calculations show that the patch volume increases when the current speed is reduced. Patch shapes as calculated by Mikhail for three current velocities are shown in figure 3. One can see that the patch dimension in the direction of the current remains essentially the same, while the dimension normal to the current increases as current speed is reduced. In fact, the maximum patch width is roughly proportional to $V^{-1/2}$, where V is the current velocity.

The effects of the release rate, R_0, the minimum detectable concentration, D_0, and the current velocity on the range of continuous release markers can be seen in figures 2 and 3. In figure 2, the range downstream is plotted as a function of concentration (in units of D_0) for a fixed ratio of R_0/D_0. If the figure is replotted in terms of R_0/D_0, the range is found to be directly proportional to R_0/D_0. Figure 3 indicates that a reduction in current velocity decreases the downstream range and increases the upstream and lateral ranges.

The amount of material required, the release rate, the cost of a 1000-hr operation, and the range were calculated for several chemical parameters. The results are in Chart 3, Section I. It is obvious that a continuous release marker is feasible only if the substance can be detected at concentrations below 0.1 ppb; otherwise, a prohibitive quantity of material will be required.

DISPOSITION OF SOURCES. To cover an area as wide as 10 mi^2, more than one marker will be required. Unfortunately, in the case of soluble markers, it is not possible to distinguish the patch of one marker from that of another. An obvious way to overcome this

*W. F. Potter, NUC, private communication.

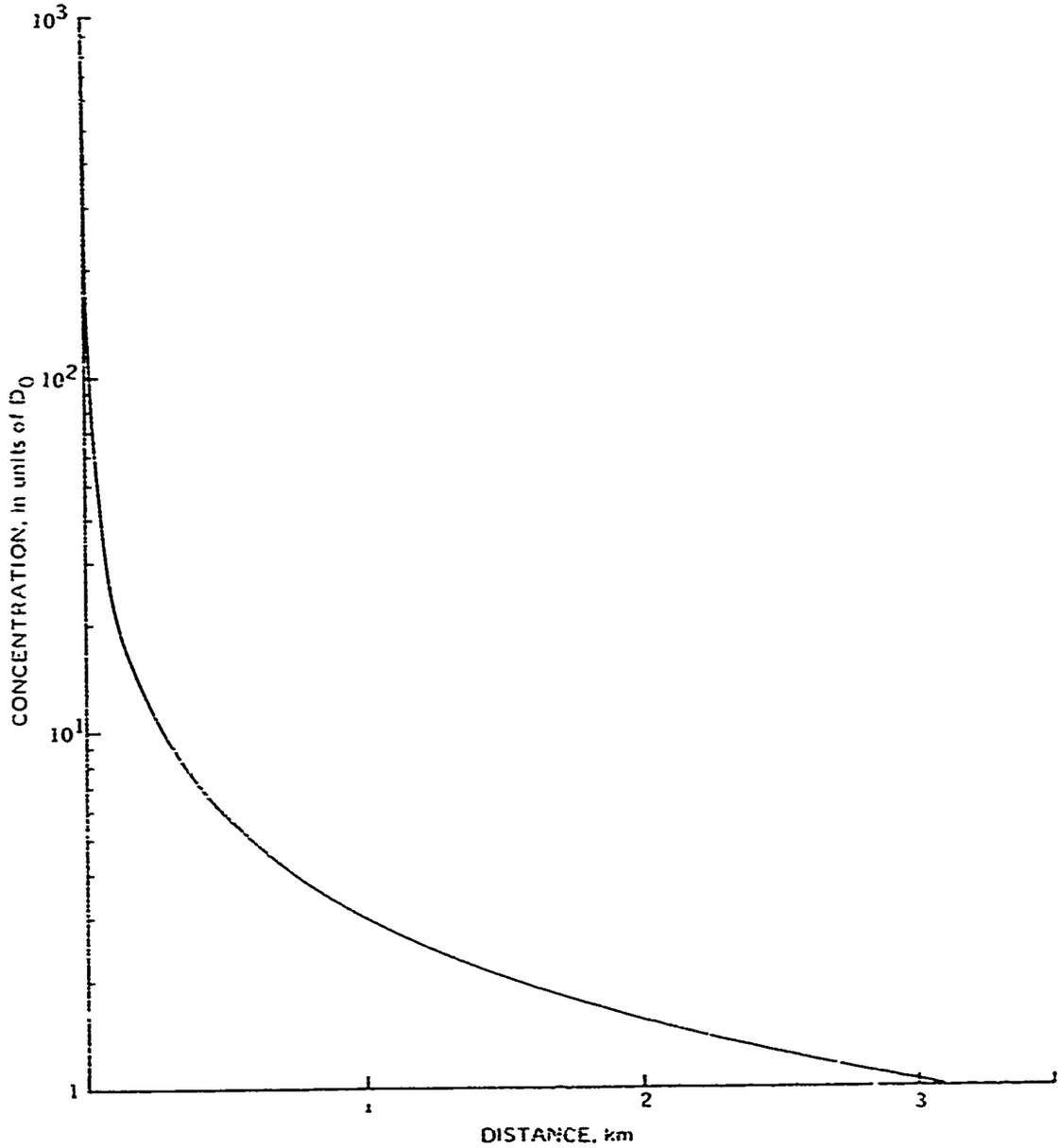

Figure 2. Concentration gradient along direction of current for continuous release under conditions listed in table 2. $Q/v_0 = 10^6$ m^3/hr.

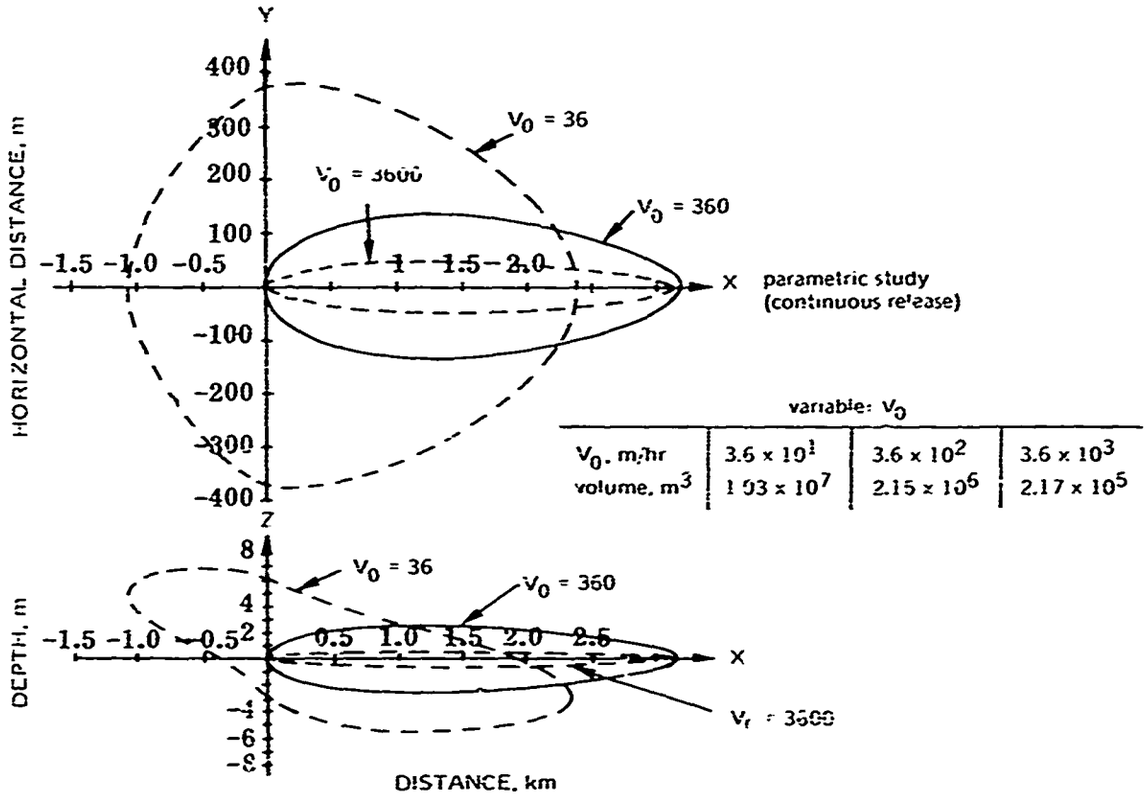

Figure 3. Effect of current velocity on patch shape for continuous release under conditions listed in table 2. $R_0 D_0 = 10^6$ m^3 hr. (Refs. 10 and 11).

disadvantage is to use a different chemical in each marker. For example, each marker could contain a different dye whose fluorescent radiation wavelength would differ from those of the other markers.

Insoluble Markers

The basic advantage of insoluble markers is that they are unaffected by water motion. Because chemicals are largely passive, however, they cannot be easily detected by probes. In addition, insoluble substances cannot be easily collected by samplers for analysis. Thus, these markers have to be stimulated by some activator, and the stimulated emission has to be detected remotely. The efficiency of such a system will depend on the range of the activator in seawater; the activator-to-marker geometry; the activation efficiency; the range of stimulated emission in seawater; and the marker-to-detector geometry.

There are three possible methods by which insoluble markers can be located: neutron activation, x-ray fluorescence, and photoluminescence.

NEUTRON ACTIVATION. A neutron source (either a radioisotope or a generator) and a gamma-ray detection system are required for this method of location. In seawater, the range of neutrons from typical sources requires that the source be placed within approximately 10 to 20 cm of the marker. Gamma rays emitted from neutron-activated markers have energies

of approximately 0.5 to 1 MeV. Half-thicknesses* for total attenuation and total absorption in water for gamma rays in this energy range are about 45 and 15 cm, respectively. Obviously, any neutron-activation system will have an extremely short range.

To obtain information of navigational value with neutron-activation insoluble marker systems, extended markers, i.e., strips laid on the bottom in a grid pattern, are required; the amount of material needed for such a system is considerable. For example, if a grid covering a 3-km x 3-km square is formed by laying strips 500 m apart, the total marker length is 14 km. Assuming 100 g of marker material per meter, a total of 14,000 kg or 15 tons of material is placed on the ocean floor.

X-RAY FLUORESCENCE. Either a radioisotopic or electron-gun x-ray source is needed for this system. The emitted radiations are x-rays of slightly lower energy than those absorbed by the marker. Unfortunately, the range of x-rays in water is so short that this method is nearly impracticable. For example, attenuation half-thickness in water for 40-keV x-rays is 2 cm. Thus, the x-ray source and detector are placed very close to the marker.

PHOTOLUMINESCENCE. Untraviolet or visible radiation can be used to stimulate photoluminescent markers. Both UV and visible light have a range of about 30 m in seawater. Thus either "point" or extended markers that photoluminesce can be readily detected on the sea floor by scanning with UV or a light source.

SUMMARY

Based on this survey of potential chemical methods for navigation systems, the following conclusions can be made.

1. Mapping of the natural chemical environment does not appear promising because there is not enough data on the variations of chemical parameters over a relatively small area of the bottom.

2. Instantaneous release of soluble markers has limited potential. The markers can only be used if the current is known and uniform and if a short-lived marker is desired.

3. Continuous release of soluble markers is a promising method if the substance can be detected at concentrations below 0.1 ppb. There are a number of inexpensive dyes which can be used for this purpose; among these dyes are Rhodamine B, Pontacyl Brilliant Pink B, Rhodamine WT, and Fluorescein.

4. A fairly wide region of the bottom can be covered by using several continuous-release markers, each of which contains a different substance.

5. An array of insoluble markers, composed of materials that photoluminesce under UV or visible light, can be used.

6. There is little data on the chemistry of the ocean bottom at depths below several thousand feet. This information is essential if man is to operate and work in this zone of the ocean.

It should be reiterated that only those chemical parameters for which *in situ* measurement systems are currently available were considered in this survey. Among the 92 natural elements, 45 are present in the ocean at concentrations below 0.1 ppb and *in situ* measurement methods are not available for most of them. In addition, there are great numbers of water soluble chemical compounds which are nonexistent in seawater and, again, for which *in situ* measurement methods have not been developed. Thus, the number of potentially useful chemical parameters can be considerably increased by developing new analytical techniques for *in situ* measurements and by improvement and/or modification of existing techniques.

** This is the thickness of a medium in which one-half of the radiation incident upon a unit area will interact with that medium.*

REFERENCES

1. R. T. Terry. *Oceanography – Its Tools, Resources and Applications.* Autonetics Report, 1 July 1961.

2. R. A. Cox, M. J. McCartney, and F. Culkin. *Deep-Sea Research.* v. 17, p. 679. 1970.

3. G. Charlot. *Colorimetric Determination of Elements.* Elsevier Publishing Co., New York. 1964.

4. G. K. Turner Associates. *Fluorimetric Studies of Pollution and Movement of Fluids.* Palo Alto, California. June 1970.

5. D. L. Feuerstein and R. E. Selleck. *J. San. Eng. Div., ASCE.* v. 89, SA4, pp. 1–21. 1963.

6. R. A. Horne. *Marine Chemistry.* Wiley Interscience, New York. 1969.

7. R. M. Garrels and C. L. Christ. *Solutions, Minerals, and Equilibria.* Harper and Row, New York. 1965.

8. *Orion Specific Ion Electrode Selection Chart.* Van Waters & Rogers Catalog.

9. *Chemical and Engineering News.* p. 87. 19 October 1970.

10. L. R. James, S. Z. Mikhail, and V. E. Schrock. *A Parametric Study of Three-Dimensional Ocean Diffusion.* Naval Radiological Defense Laboratory Report, NRDL-TR-69-50. 1969.

11. S. Z. Mikhail and L. R. James. *Implications of Substitution of Strontium Oxide for Strontium Titanate in Terrestrial/Marine Radioisotope Power Units.* Naval Radiological Defense Laboratory Report, NRDL-TR-69-75. 1969.

THE DETECTION RANGE OF EXTREMELY-LOW-FREQUENCY ELECTROMAGNETIC WAVES IN THE SEA

by

N. Booth
NUC

CONTENTS

THE DETECTION RANGE OF EXTREMELY-LOW-FREQUENCY ELECTROMAGNETIC WAVES IN THE SEA

INTRODUCTION

The propagation of electromagnetic (EM) radiation in the sea is considerably different from its propagation in air. Seawater is an electrical conductor that severely attenuates EM waves which deliver their energy to the charged ions. The electric field of a plane wave in seawater has the form (ref. 1)

$$E = E_0 e^{-(1+j)x/\delta} , \tag{1}$$

where δ is the attenuation length given by

$$\delta = \sqrt{\frac{1}{\pi f_0 \mu \sigma}} = \frac{250}{\sqrt{f}} \text{ m} . \tag{2}$$

where f_0 is the wave frequency, $\mu = 4\pi \times 10^{-7}$ H/m is the permeability of seawater and free space, and $\sigma = 4$ (ohm m)$^{-1}$ is the conductivity of seawater. In a distance of 1 attenuation length, the wave's energy is attenuated by 9 dB.

The greatest ranges of detection will be obtained for long attenuation lengths which occur in the extremely-low-frequency (ELF) range ($1 < f < 100$ Hz).

This article will predict an upper bound to the expected range for practical sources in the ELF range where the attenuation length is $25 \text{ m} < \delta < 250$ m. The range of detection will depend upon the parameters which are outlined below and examined in greater detail in the following sections.

POWER. Range depends on the power radiated by the source, which is assumed to be 10 W, i.e., P = 10 W.

ANTENNA CONFIGURATION. The coupling efficiency of the available power to the wave fields will depend on the type and size of the antenna. In the section, *Comparison of Electric Antennas*, the common underwater electric antennas are examined, and results show that the short-circuited coaxial electric dipole antenna couples best to the wave fields in seawater. This antenna is used in this article with the assumption that its length is 10 m. Longer antennas have better coupling; however, 10 m is the longest length that is of practical use. In the section, *Magnetic Dipole Radiation in the Deep Ocean*, the range of detection from a magnetic-loop antenna is shown to be approximately equal to the range for the short-circuited electric dipole antenna.

FREQUENCY. The most sensitive dependence on frequency is through the attenuation length. Noise and the coupling of an antenna to fields in seawater are also dependent on frequency. The short antennas previously mentioned couple better to fields at higher frequencies.

The analysis in the section, *Electric Dipole Radiation in the Deep Ocean*, shows that the best frequencies are in the ELF range.

NOISE. In the section, *Signal Detection and Noise in the Sea*, the sources of EM noise in the ocean are examined. It is concluded that atmospheric noise within a few attenuation lengths of the surface dominates the results. Below this depth, detection is limited by receiver sensitivity. The ranges obtained are extremely sensitive to the assumptions concerning the noise spectrum.

DEPTH. At depths less than an attenuation length, the underwater antenna can couple to surface waves which propagate unattenuated through the air. The main propagation loss is attenuation in the paths between the source and the surface and the receiver and the surface.

HEIGHT ABOVE BOTTOM. Near the bottom, the submerged antenna couples to bottom fields which propagate with less attenuation than in the water. In the average bottom, the attenuation length is longer by a factor of approximately 6. The ranges obtained for propagation near the bottom are sensitive to the bottom-conductivity value which can vary by an order of magnitude depending on the type of bottom material.

OBSERVATION TIME. The coherent detection of signals in noise is also discussed in this article. The detection of a signal in noise is improved if the bandwidth of the detector is very narrow, which is equivalent to observing the signal for a long time. It is assumed that the observation time is a maximum of 100 sec, producing a bandwidth of 10^{-2} Hz.

The results of the computations are in tables 1 through 3. These ranges, which are order-of-magnitude estimates for the best source-receiver orientation, represent the distance from the source at which the signal-to-noise ratio for coherent detection is unity for the observation of 100 sec.

PLANE WAVES ABOVE, IN, AND BELOW THE SEA

The detection range of EM waves from sources in the sea is related to the characteristic properties of plane-wave propagation in the air, the sea, and the ocean bottom.

The electric fields of plane waves in a conducting dielectric medium have the following dependence on time, t, and position, x:

$$E = E_0 e^{\mp j(\omega t - kx)}, \tag{3}$$

where ω is the angular frequency and k is the complex propagation constant given by the dispersion relation (ref. 1):

$$k^2 = \omega\mu(\omega\epsilon + j\sigma), \tag{4}$$

where μ, ϵ, and σ are the permeability, permittivity, and conductivity of the medium, respectively.

In air, $\sigma/\omega\epsilon \ll 1$, and k is real and given by

$$k_a = \frac{2\pi}{\lambda_a} = \frac{\omega}{c}, \tag{5}$$

where λ_a is the wavelength in air and c is the speed of light.

In and below the sea for frequencies below 1 MHz, $\sigma/\omega\epsilon \gg 1$ and k is complex and given by

$$k = (1 + j)/\delta_{w,b} \quad (6)$$

The attenuation length, $\delta_{w,b}$, is given by

$$\delta_{w,b} = \sqrt{\frac{2}{\omega\mu\sigma_{w,b}}}, \quad (7)$$

where $\sigma_{w,b}$ is the conductivity of the water or bottom. In this case, the electric field of a plane wave has the form

$$E = E_0 e^{j(\omega t - x/\delta)} e^{-x/\delta} \quad (8)$$

At a distance of 1 attenuation length, the field strength is down by 4.3 dB.

The attenuation lengths in seawater and in the ocean floor are plotted as a function of frequency in figure 1. The conductivity of seawater is assumed to be $\sigma_w = 4$ mho/m (ref. 1), and the conductivity of the bottom is assumed to be $\sigma_b = 0.1$ mho/m (ref. 1). Also plotted for air is $\lambda_a/2\pi$. For the ranges, r, of interest

$$\frac{\lambda_a}{2\pi} \gg r > \delta_b > \delta_w \quad (9)$$

Using Maxwell's equations for a plane wave, it can be shown that the magnetic field is related to the electric field by the intrinsic impedance of water

$$\frac{|E|^2}{|H|^2} = \frac{\omega\mu}{\sigma} \quad (10)$$

This relationship is true for all fields which are more than a wavelength away from the source.

COMPARISON OF ELECTRIC ANTENNAS

Fields, which are at a great distance compared with the antenna's size, are the same as fields from a point dipole antenna with an equivalent dipole moment that is characteristic of the antenna. The electric fields are proportional to this dipole moment. In this section, the equivalent dipole moments for the common underwater antennas are compared; results show that the short-circuited coaxial dipole antenna has the best coupling to the ocean medium and generates the largest dipole moment and radiation fields.

Biconical Antenna

The biconical antenna consists of two coaxial cones with their apices together at the origin. Moore (ref. 2) has calculated the equivalent dipole moment and characteristic resistance.

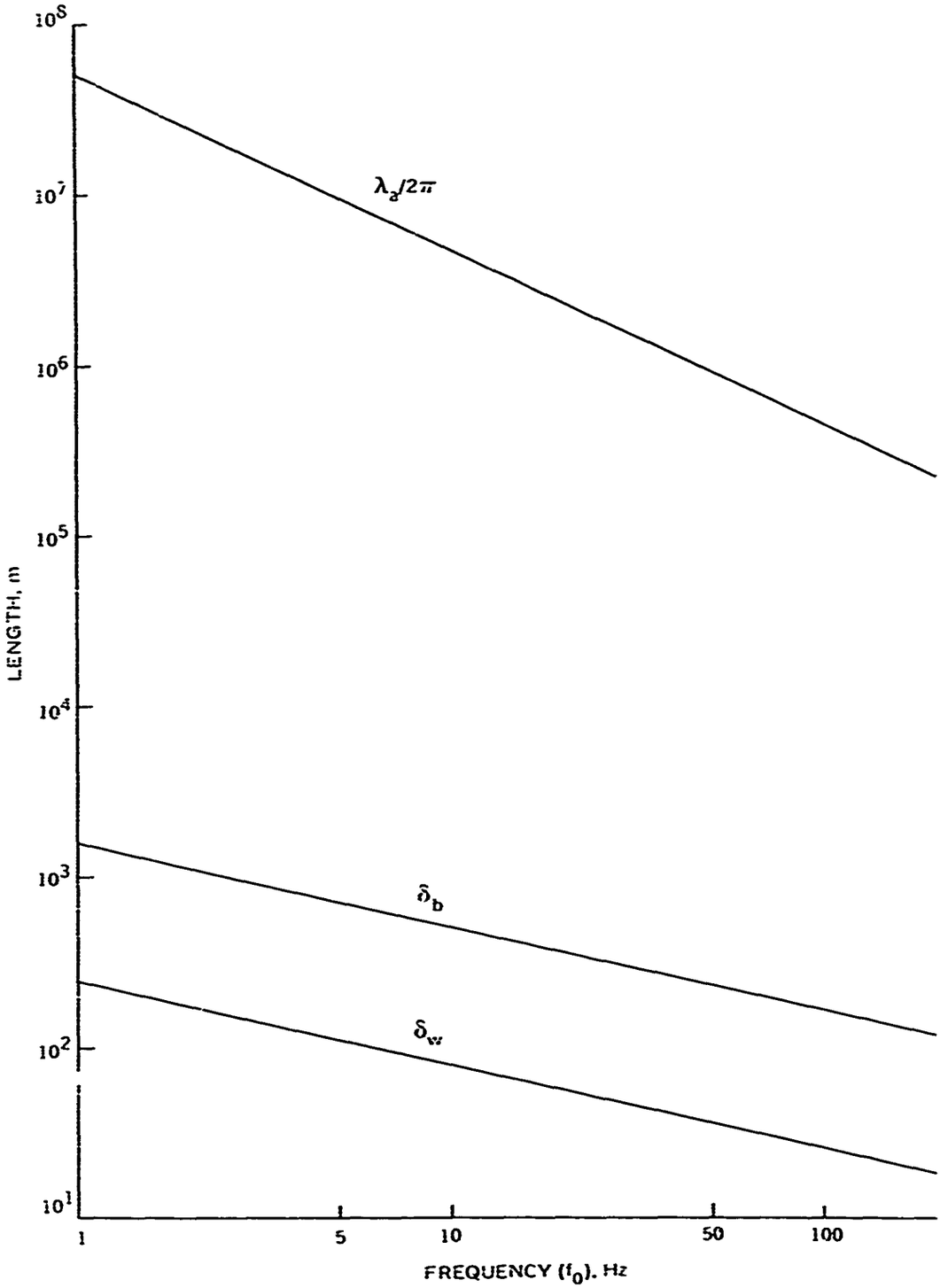

Figure 1. Characteristic lengths as a function of frequency.

For an input power, P, the dipole moment for a biconical antenna is

$$p_{bic} = 2I_0 l \cos\theta_0 = \frac{2\sqrt{P}\, l \cos\theta_0}{\sqrt{N/\pi}\, \log \cot \theta_0/2}, \tag{11}$$

where θ_0 is the cone angle, l is the length along the cone's surface, and $N = \sqrt{\omega_0 \mu / \sigma_w}$ is the intrinsic impedance of seawater. For P = 10 W, l = 3 m, θ_0 = 30 deg, f = 10 Hz:

$$p_{bic}^{30\ deg} = 580\ A\ m\ . \tag{12}$$

For θ = 10 deg,

$$p_{bic}^{10\ deg} = 490\ A\ m\ . \tag{13}$$

The dependence on θ_0 is not critical for practical values in the range 10 deg < θ_0 < 50 deg.

Coaxial Antennas

The coaxial antenna is an insulated wire with seawater as the outer conductor. It has two practical configurations: short circuited to the water at each end or open circuited with the insulator covering each end. Moore analyzed these antennas and obtained the following equivalent dipole moments when the insulation thickness was small when compared with the attenuation length in water.

For an input power, P, the dipole moment for the short-circuited dipole antenna is given by (ref. 2)

$$p_{sc} = \sqrt{\frac{8PI}{\omega\mu}} = 1700\ A\ m \tag{14}$$

for P = 10 W, l = 3 m, f = 10 Hz.

The dipole moment for the open-circuited dipole antenna is given by (ref. 2)

$$p_{oc} = \sqrt{\frac{6PI}{\omega\mu}} = 1480\ A\ m \tag{15}$$

for the above parameters.

Comparison of Electric Antennas

The ratio of the equivalent dipole moments for the short- and open-circuited coaxial antennas is

$$\frac{p_{sc}}{p_{oc}} = \sqrt{\frac{4}{3}} \gtrsim 1\ . \tag{16}$$

which is independent of all parameters. The short-circuited antenna has slightly better coupling with the radiation fields.

The ratio of the dipole moments for the short-circuited coaxial and biconical antennas is

$$\frac{p_{sc}}{p_{bic}} = \sqrt{\frac{2}{\pi l \sqrt{\omega\mu\sigma}}} \approx 3 . \tag{17}$$

At higher frequencies, the biconical antenna will have a greater dipole moment and a larger radiation field; however, the losses due to attenuation at higher frequencies more than offset the increase in the dipole moment.

These results show that the short-circuited coaxial antenna provides the best coupling to the ocean medium. It is used in all calculations of electric dipole fields.

SIGNAL DETECTION AND NOISE IN THE SEA

Electromagnetic noise in the sea comes from three known sources.

1. The propagation and attenuation of natural atmospheric noise at the depth of the receiver.
2. Noise generated by turbulence coupled with the magnetic field of the earth.
3. Thermal or Johnson noise in the receiver which limits the receiver's sensitivity.

These sources are the limiting factors which determine the detection range of a given source configuration. In this section, the detection of signals in a noisy environment is examined, and the sources of noise and the depths in the ocean where each is dominant are discussed.

Detection in a Noisy Environment

Assume that the signal is at frequency ω_0. A coherent phase-locked detection system will be used, and the signal will be observed for a time, T. After this time, it will be decided if the signal has been detected by determining if the detector registers a signal greater than the noise level, i.e., if the signal-to-noise level is greater than one.

The signal-to-noise ratio for coherent detection is given by (ref. 3)

$$d^2 = \int_{-\infty}^{\infty} \frac{S^2(\omega)}{N(\omega)} \frac{d\omega}{2\pi} . \tag{18}$$

where $N(\omega)$ is the power spectrum of the electric noise in V^2/m^2 Hz and $S(\omega)$ is the field spectrum of the signal. Because the cw signal is observed for a time T, the received electric field is given by

$$E(t) = \begin{cases} E_0(r,\omega_0)e^{-j\omega_0 t} & 0 < t < T \\ 0 & \text{otherwise} \end{cases} \tag{19}$$

where r is the distance from the source. $S(\omega)$ is given by the Fourier transform of E(t):

$$S(\omega) = E_0(r,\omega_0)\frac{e^{-j(\omega-\omega_0)T}-1}{-j(\omega-\omega_0)}. \tag{20}$$

Thus,

$$S^2(\omega) = E_0^2(r,\omega_0)4\frac{\sin^2(\omega-\omega_0)T/2}{(\omega-\omega_0)^2}. \tag{21}$$

Because $S^2(\omega)$ is peaked at $\omega=\omega_0$ and is of width 1/T, it is assumed that $N(\omega) = N(\omega_0)$ is constant over this range. For $T > 1/2\pi\omega_0$, this assumption is very good. On performing the ω integration, the signal-to-noise ratio becomes

$$d^2 = \frac{TE_0^2(r,\omega_0)}{N(\omega_0)}. \tag{22}$$

The value of $E_0^2(r)$ for marginal detection is determined by setting the signal-to-noise ratio equal to unity:

$$E_0^2 = \frac{N(\omega_0)}{T}. \tag{23}$$

A similar calculation gives the magnetic field for marginal detection in magnetic noise:

$$H_0^2 = \frac{M(\omega_0)}{T}, \tag{24}$$

where $M(\omega_0)$ is the magnetic-noise spectrum.

Atmospheric Noise

Lightning is the main source of atmospheric FM noise in the 1- to 100-Hz range. When these waves propagate over the ocean, they are strongly affected by the boundary conditions at the surface. Above a perfect conductor, only the normal electric field and the tangential magnetic field exist. Seawater is not a perfect conductor, but noise at the surface is considerably different from noise over land.

Soderberg and Finkle (ref. 4) have measured ELF atmospheric noise above and in the sea. In their paper, they discuss the coupling of noise above the sea to that below the surface. They have measured the noise spectrum in the 5- to 500-Hz range at a 23-m depth. Their data will be extrapolated in this section to apply to various depths. Their data fits the approximate form

$$N_h(\omega_0) = \begin{cases} \dfrac{10^{-16}}{f_0^2}\, e^{-2h/\delta} & f_0 < 10 \text{ Hz} \\ \dfrac{3.2 \times 10^{-18} e^{-2h/\delta}}{\sqrt{f_0}} & 10 \text{ Hz} < f_0 < 100 \text{ Hz} \end{cases} \tag{25}$$

The magnetic-noise spectrum $M_h(f_0)$, is related to $N_h(f_0)$ by the intrinsic impedance of water (Eq. 10)

$$M_h(\omega_0) = \frac{\sigma}{\omega_0 \mu}\, N_h(\omega_0)\,. \tag{26}$$

System Noise

The best receiving system that can be constructed will be limited in its sensitivity by thermal noise. This noise will be calculated and used to obtain an upper limit on the detection range. It should be emphasized, however, that this limit in receiver sensitivity is difficult to achieve in practice.

The thermal-noise voltage induced in an antenna is given by (ref. 5)

$$V = \sqrt{\frac{4\theta R}{T}}\,, \tag{27}$$

where θ is the temperature measured in joules, R is the input resistance, and T is the measuring time. The electric field at an electric antenna is given by

$$E = \frac{V}{l}\,,$$

where l is the length of the antenna.

With the use of Eq. 23, the equivalent electric-noise spectrum can be calculated:

$$N_j(\omega_0) = TE^2 = \frac{TV^2}{l^2} = \frac{4\theta R}{l^2}\,.$$

For a short-circuited coaxial electric dipole antenna, R is given by (ref. 2)

$$R = \frac{\omega_0 \mu l}{8} + R_w\,.$$

where R_w is the resistance of the wire in the antenna. The noise spectrum of the receiver is smallest when R_w is negligible and is given by

$$N_j(\omega) = \frac{\theta\omega_0\mu}{21} \quad . \tag{28}$$

At normal water temperatures (300 °K) and for l = 10 m,

$$N_j(f_0) = 1.7 \times 10^{-27} f_0 \ V^2/m^2 \ Hz. \tag{29}$$

At 10 Hz, this theoretical minimum noise is 10^5 times lower than the noise in the system used by Soderberg and Finkle in their atmospheric-noise measurements. The predictions of range using this limit will be an upper bound for the ranges obtained in actual measurements.

The magnetic-noise spectrum for a magnetic dipole antenna can also be calculated. The voltage (Eq. 26) induces a magnetic field in the loop given by

$$V = \omega_0\mu N\pi a^2 H \ , \tag{30}$$

where a is the radius of the loop and N is the number of turns. The equivalent magnetic-noise spectrum can be calculated using Eq. 24:

$$M_j(\omega_0) = TH^2 = \frac{N^{-2}TV^2}{\omega_0^2\mu^2\pi^2a^4} = \frac{4\theta RN^{-2}}{\omega_0^2\mu^2\pi^2a^4} \quad . \tag{31}$$

For a magnetic dipole antenna, the input resistance, R, is given by (ref. 2)

$$R = \frac{2\omega^2\mu^2\sigma a^3N^2}{3} \tag{32}$$

and the magnetic-noise spectrum is given by

$$M_j(\omega_0) = \frac{8\theta\sigma}{3\pi^2a} \quad . \tag{33}$$

A comparison with Eq. 26 shows that

$$M_j(\omega_0) = \frac{161}{3\pi^2a} \frac{\sigma}{\omega\mu} \ N_j(\omega_0) \ . \tag{34}$$

The factor $3\pi^2a/161 \approx 1$ so that the ratio of magnetic to electric noise is approximately the same for both system and atmospheric noise.

Water Turbulence

The noise from water turbulence is generated by that component of water flow perpendicular to the earth's magnetic field. The electric field is given by

$$E(t) = v(t)B_0 ,$$

where v(t) is the velocity perpendicular to the earth's magnetic field, B_0.

This electric field is polarized in a direction perpendicular to B_0, and it has no magnetic component because the field is in the same vicinity as the source. This noise, which can be discriminated against with a magnetic dipole antenna, will not be considered as an important noise source.

Comparison

At shallow depths, atmospheric noise will dominate and limit the range of detection. For a wave frequency of 10 Hz, thermal noise will equal atmospheric noise at a 720-m depth. Below this depth, the range will be maximum and limited by receiver noise. Figure 2 is a plot of depth as a function of frequency for which the atmospheric and thermal noise are equal.

ELECTRIC DIPOLE RADIATION IN THE DEEP OCEAN

Radiation from a short-circuited dipole antenna in seawater of infinite extent will be discussed in this section. Graphs are presented from which the detection range of the signal can be determined as a function of frequency, source power, antenna length, noise level, and observation time.

Cylindrical geometry in which the dipole is aligned along the z axis at r = 0 will be used (fig. 3). The surface and bottom are assumed to be a few attenuation lengths from the source. Because the largest radiated fields are at z = 0, the range for the receiver will be calculated at z = 0. The dominant electric field is in the z direction and is given by (ref. 1)

$$|E_z|^2 = \frac{p^2\omega_0^3\mu^3\sigma}{32\pi^2}\,\frac{e^{-2R}}{R^2} , \tag{35}$$

where

$$R = r/\delta_w > 1 \tag{36}$$

is the range measured in water attenuation lengths and p is the equivalent dipole moment of the antenna. The magnetic field, in the φ direction, is related to the electric field by the intrinsic impedance

$$\frac{|E_z|^2}{|H_\varphi|^2} = \frac{\omega_0\mu}{\sigma} . \tag{37}$$

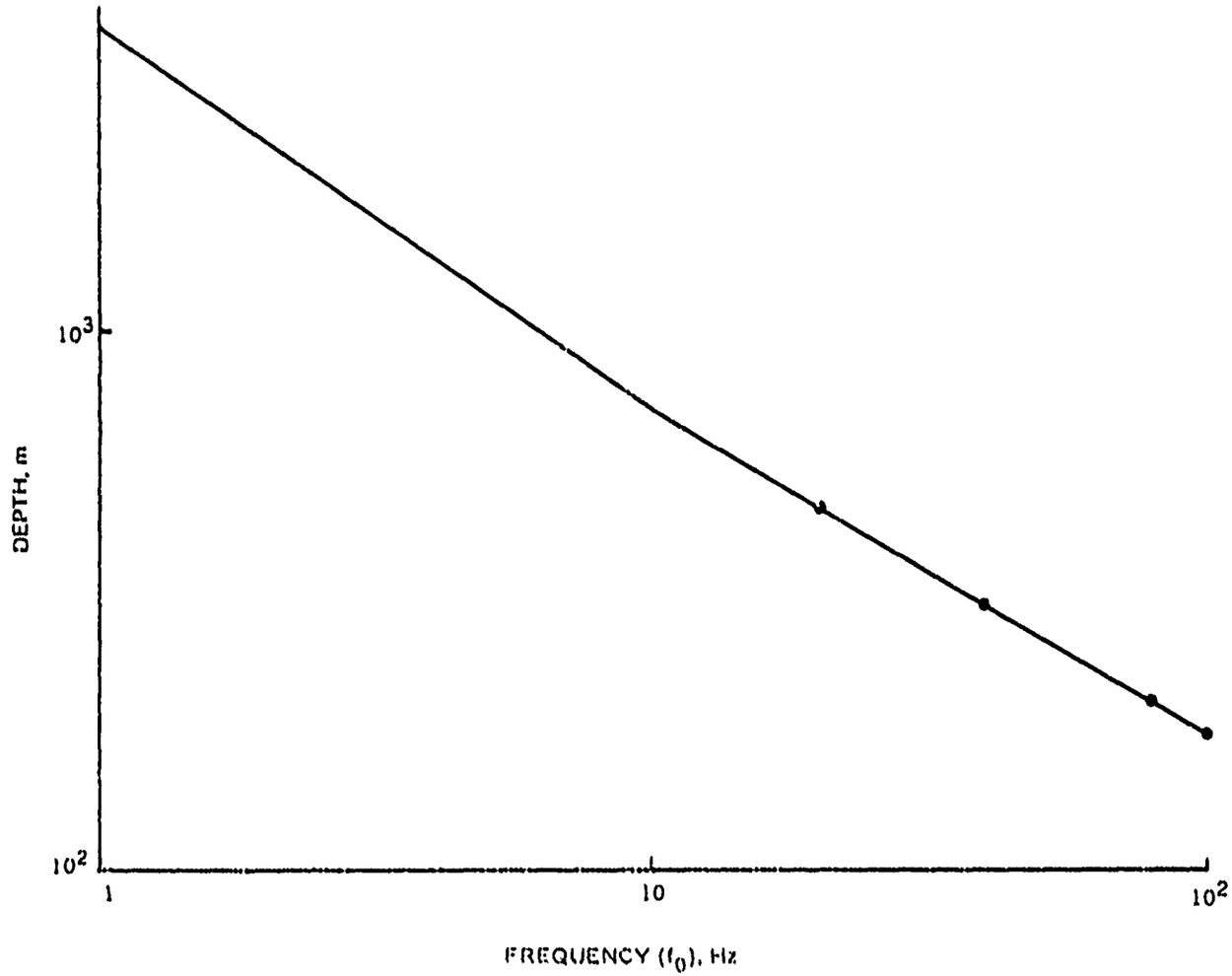

Figure 2. Depth at which receiver noise equals atmospheric noise.

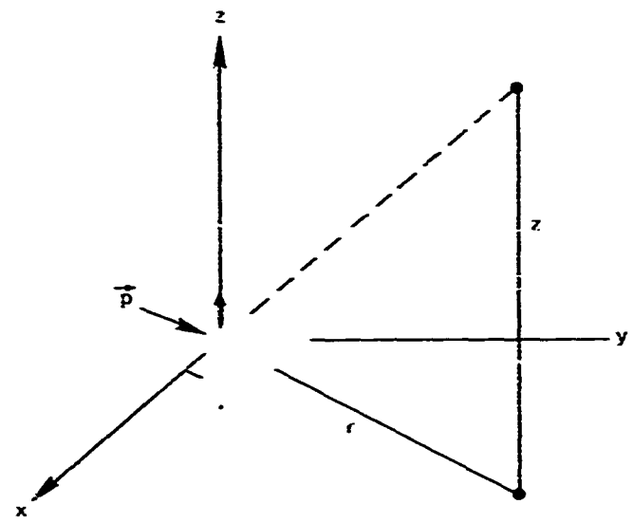

Figure 3. Cylindrical geometry.

For the short-circuited coaxial antenna, p is given by Eq. 14. Eq. 35 thus becomes

$$|E_z|^2 = \frac{Pl\omega_0^2\mu^2\sigma}{4\pi^2}\,\frac{e^{-2R}}{R^2} \quad . \tag{38}$$

where P is the input power and l is the length of the antenna. For marginal detection, $|E_z|^2$ is given by Eq. 23:

$$\frac{4\pi^2 N(\omega_0)}{TPl\omega_0^2\mu^2\sigma} = \frac{e^{-2R}}{R^2} \quad . \tag{39}$$

The right-hand side of Eq. 39 is a function only of the normalized range. It will be designated by

$$F_i(R) = \frac{e^{-2R}}{R^2} \quad .$$

where the subscript i designates this function for the infinite medium case. The left-hand side of Eq. 39 is a function of frequency, the product TPl, and the depth through the dependence of the noise. It is designated by the function

$$G_i(TPl, a, f_0) = \frac{4\pi^2 N(\omega_0)}{TPl\omega_0^2\mu^2\sigma} \quad . \tag{40}$$

Using the atmospheric-noise spectrum from Eq. 25, the function $G_i(TPI, h, f_0)$ is plotted as a function of frequency in figure 4 for TPI = 10^4 W sec m and h = 0, 400, 800 m. G_i is also plotted for the deep ocean where the system noise of Eq. 29 dominates. In addition, $F_i(R)$ is plotted as a function of R in figure 4. To determine range at a given frequency, f_0, the R is found for which $G_i(f_0) = F_i(R)$ which, in turn, gives the range in attenuation lengths. Figure 1 can be used to convert R to a range in meters.

The maximum ranges possible, found by using the curve for G_i (system noise), are obtained at depths below those in figure 2. The curve for the range at the surface ($G_i(0)$) is included as an upper bound on G_i. Within a few attenuation lengths of the surface, the range will be longer and the results from the section, *Dipole Radiation Near the Surface*, should be used. If the source and receiver are near the bottom, the ranges will also be longer than those in this section, and the results from the section, *Dipole Radiation Near the Bottom*, should be used.

Table 1 is a summary of ranges obtained in the ocean far from the surface and the bottom.

Table 1. Range in the Infinite Medium Approximation.

TPI = 10^4 W sec m.

	Depth (h), m	Frequency (f), Hz	$R(\delta_w)$	Range, m
	0	10	12.5	1000*
	0	100	16.7	260*
	400	4	13.5	1700
	400	10	17	1360
	800	4	16.3	2000
system-noise limited	>1300	4	19	2400
	> 720	10	20	1600
	> 180	100	22	330

*See section, *Dipole Radiation Near the Surface*

MAGNETIC DIPOLE RADIATION IN THE DEEP OCEAN

Radiation from a magnetic dipole is similar to that from an electric dipole with the electric and magnetic fields interchanged. The fields, maximum at $z = 0$ (see fig. 3), are given by (ref. 1)

$$|H_z|^2 = \frac{m^2}{32\pi^2}\,\omega^3\mu^3\sigma^3\,\frac{e^{-2R}}{R^2}\,. \tag{41}$$

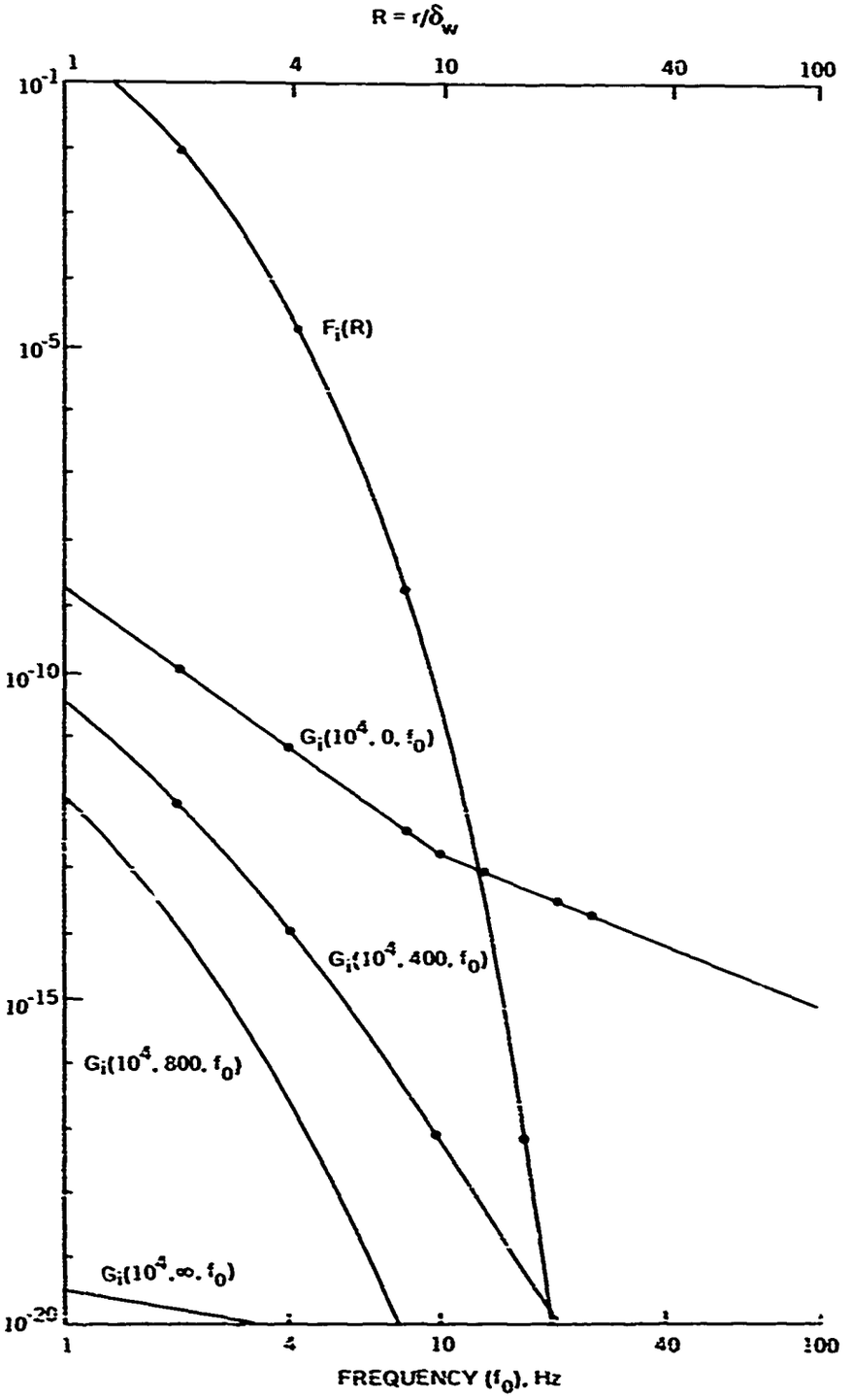

Figure 4. Propagation functions F_i and G_i for infinite medium approximation.

where

$$R = r/\delta_w > 1$$

and m is the magnetic dipole moment. The magnetic field is related to the electric field by the intrinsic impedance

$$\frac{E^2}{H^2} = \frac{\omega\mu}{\sigma} .$$

The equivalent magnetic moment, m, for a loop antenna of radius a, has been calculated by Moore (ref. 2)

$$m^2 = \frac{3\pi^2 Pa}{2\omega^2\mu^2\sigma} . \tag{42}$$

H_z^2 then becomes

$$|H_z|^2 = \frac{3Pa\omega\mu\sigma^2}{64} \frac{e^{-2R}}{R^2} . \tag{43}$$

Using the fact that magnetic noise is given by

$$M(\omega_0) = \frac{\sigma}{\omega\mu} N(\omega_0) , \tag{44}$$

the following is obtained for marginal detection:

$$\frac{64}{3} \frac{N(\omega_0)}{Pa\omega^2\mu^2\sigma T} = F_i(R) = \frac{16}{3\pi^2} \frac{1}{a} G_i(TPI, h, f_0) . \tag{45}$$

For practical antennas, the factor

$$\frac{16}{3\pi^2} \frac{1}{a} \approx 1 ,$$

and the ranges obtained are almost identical to those obtained for the electric dipole antenna. When a magnetic detector is used in the system-noise-limited region, the exact equation (Eq. 39) results. This is not surprising when the symmetry between the electric and magnetic fields and the noise in far-field ranges of the sources are considered.

DIPOLE RADIATION NEAR THE SURFACE

When the source and receiver are at a depth much less than the range predicted for dipole radiation in the deep ocean, the range of propagation is considerably increased. In subsurface-to-subsurface propagation, energy follows an up-over-down path, and the wave suffers exponential attenuation in the up-and-down portions of the path. In air where the wavelength is very long, geometrical losses dominate.

The problem of electromagnetic waves near the surface has been investigated by Moore (ref. 2) and Baños and Wesley (ref. 6). Their results are summarized by Kraichman (ref. 1). For propagation in and above seawater, the formulas in table 3.7 of Kraichman are applicable. In this section, the geometry of figure 3, with the air-water interface at a height, h, above the origin, will be used. Formulas are given for the electric and magnetic dipoles aligned in the vertical (z) direction and in the horizontal ($\varphi = 0$) direction. Comparison of the field formulas shows the following characteristics for distances $r \ll \lambda$ air.

Vertical Electric Dipole (VED)

For the VED, the electric field in the $\hat{r}$ direction, E_r, is larger than the fields in the other directions by a factor of $r/\delta_w \geq 1$. The only magnetic field is in the $\hat{\varphi}$ direction, and it is related to E_r by

$$\frac{|E_r|^2}{|H_\varphi|^2} = \frac{\omega\mu}{\sigma} .$$

This ratio is the same as the ratio of the noise; thus, the ranges of both fields are equal.

Horizontal Electric Dipole (HED)

For the HED, the horizontal components of the electric field dominate the z component by a factor of approximately

$$\frac{\lambda^2_{air}}{\lambda_w r} \gg 1 .$$

The horizontal components of the magnetic field dominate H_z by

$$\frac{r}{\delta_w} > 1 .$$

The ratio of the horizontal electric field to the horizontal magnetic field is given by

$$\frac{|E_r|^2}{|H_\varphi|^2} = \frac{\omega\mu}{\sigma} .$$

Thus, ranges of both fields are equal.

VED and HED Comparison

The ratio of the dominant electric fields in the VED and HED cases is given by

$$\frac{|E_r|^2_{HED}}{|E_r|^2_{VED}} \cong \frac{\lambda_a^2}{\lambda_w^2} \gg 1 .$$

Thus, the HED has the larger field at a distance r. This orientation provides the greatest range, and it will be used in this section to calculate the expected range.

Range will be calculated using two assumptions: (1) the source is a horizontal dipole aligned along the direction $\varphi = 0$, and (2) the receiver is at the same depth and is aligned to receive the greatest electric field. The magnitude of this electric field has a very weak dependence on φ and is given by (ref. 1)

$$|E^2| = \frac{p^2\omega_0^3\mu^3\sigma}{8\pi^2} \frac{e^{-4h/\delta_w}}{R^6} \left(\frac{\cos^2\varphi}{4} + \sin^2\varphi\right) . \tag{46}$$

where $R = r/\delta_w$ and we assume that $r/\lambda_{air} \ll 1$. Using the equivalent dipole moment for a short-circuited dipole antenna (Eq. 14) and choosing $\varphi = \pi/2$, the following is obtained:

$$|E|^2 = \frac{PI\omega_0^2\mu^2\sigma}{\pi^2} \frac{e^{-4h/\delta_w}}{R^6} . \tag{47}$$

For marginal detection, $|E|^2$ is given by Eq. 23:

$$\frac{\pi^2 N(\omega_0) e^{4h/\delta_w}}{TPI\omega_0^2\mu^2\sigma} = \frac{1}{R^6} . \tag{48}$$

The functions $G_s(TPI, h, \omega_0)$ and $F_s(R)$, analogous to G_i and F_i for the infinite medium case, are given by

$$G_s(TPI, h, f_0) = \frac{\pi^2 N(\omega_0) e^{4h/\delta_w}}{TPI\omega_0^2\mu^2\sigma} \tag{49}$$

$$F_s(R) = 1/R^6 .$$

where s designates the functions for propagation near the surface.

Because these calculations are for radiation near the surface, the atmospheric noise will dominate and Eq. 25 will be used for $N(\omega_0)$.

$F_s(R)$ is plotted as a function of $R = r/\delta_w$ in figure 5. $G_s(f_0)$ is also plotted as a function of frequency for depths h = 0 and 100 m and TPI = 10^{-4} W m sec. To find the range at a

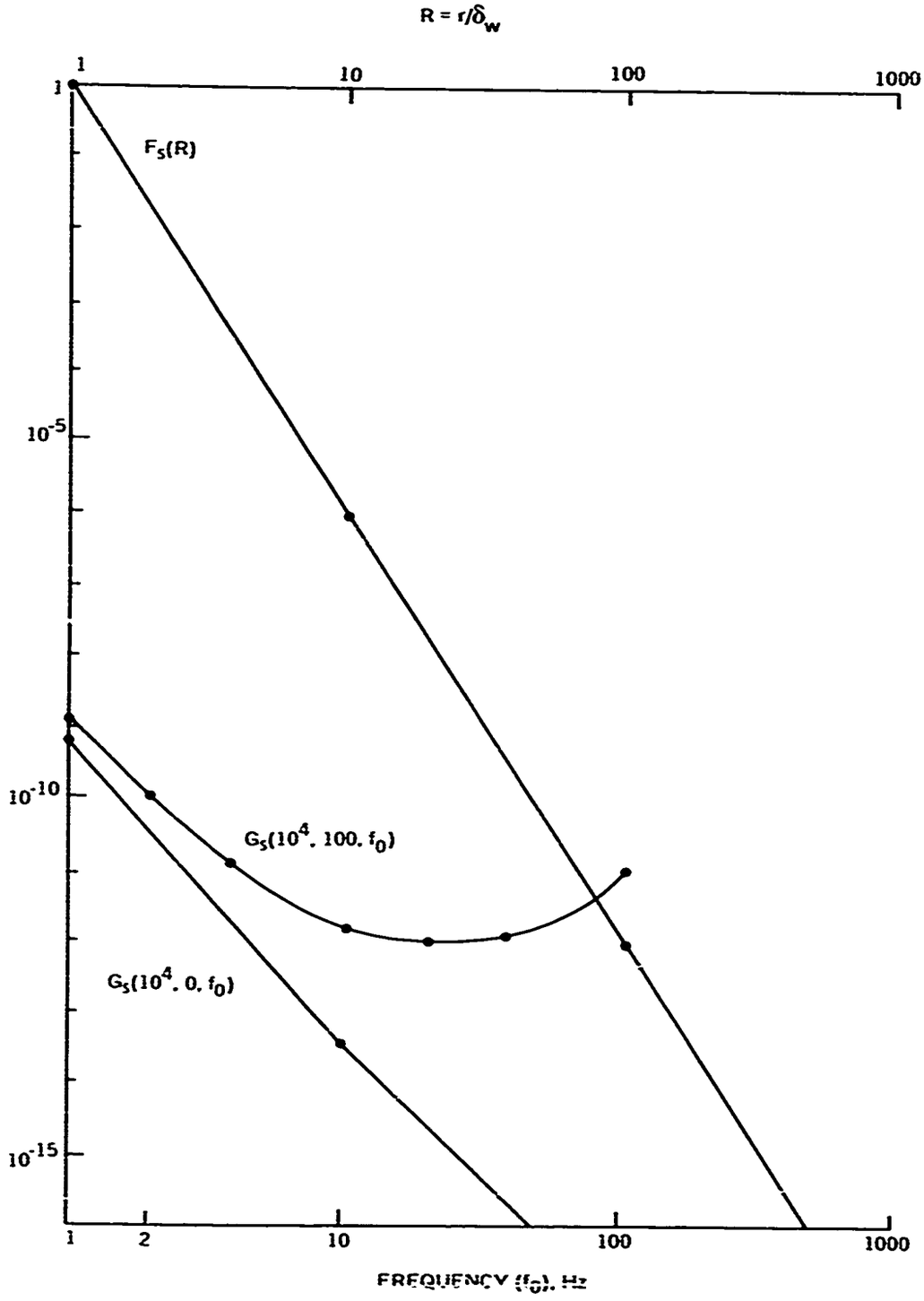

Figure 5. Functions $F_s(R)$ and $G_s(TH, h, f_0)$ for propagation near the surface.

given frequency, f_0, the R at which $F_s(R) = G_s(f_0)$ is determined. R is the range measured in units of δ_w, which can be converted into meters by using figure 1. Table 2 is a summary of the ranges obtained near the surface.

Table 2. Summary of Ranges Obtained Near the Surface.

Depth (h), m	Frequency (f), Hz	R	Range, m
0	4	90	11,250
0	10	170	13,600
0	100	750	19,000
100	4	63	7900
100	10	95	7600
100	100	70	1700

An analysis of magnetic dipoles aligned vertically and horizontally shows that the horizontal orientation has the larger fields and that the ranges obtained are approximately the same as ranges for the horizontal electric dipole. As previously stated, the difference in the function G is a factor of $161/(3\pi^2 a) > 1$.

DIPOLE RADIATION NEAR THE BOTTOM

The problem of dipole radiation near the bottom is similar to the problem of radiation near the surface. The main differences are listed below.

1. The wave is exponentially attenuated in the path through the bottom, while there is no attenuation through the air.

2. The wavelength in the bottom is much longer than the wavelength through water so that the formulas presented by Kraichman (ref. 1, table 3.7) are applicable. The range near the bottom will be shorter than the range near the surface, but longer than the range in the deep ocean.

The analyses of the relative size of the field strengths for vertical and horizontal electric dipoles, similar to those previously discussed, have the following results.

1. The dominant electric fields from the VED and HED are in the horizontal plane parallel to the bottom.

2. The electric field from an HED source is larger than the field from a VED source by the factor $r/\delta_b > 1$. The best ranges will be obtained from an HED source.

In the calculation of range at the bottom, it will be assumed that the source is a horizontal electric dipole aligned along the direction $\varphi = 0$. It will also be assumed that both the source and receiver are on the bottom and that the receiver is aligned to receive the largest electric field. This field is given by

$$|E^2| = \frac{p^2 \omega_0^3 \mu^3 \sigma_b^3}{32\pi^2 \sigma_w^2} \frac{e^{-2R_b}}{R_b^2} \left(\frac{\cos^2\varphi}{4} + \frac{\sin^2\varphi}{R_b^2} \right). \tag{50}$$

where $R_b = r/\delta_b > 1$ is the range in units of the attenuation length in the bottom. Using the dipole moment for the short-circuited coaxial antenna (Eq. 14) and using Eq. 23 for the value of the electric field for marginal detection, the following is obtained:

$$G_b(TPI, f_0) = F_b(R_b, \varphi) \ , \tag{51}$$

where

$$G_b(TPI, f_0) = \frac{\pi^2 \sigma_w^2 N(\omega)}{TPI \omega^2 \mu^2 \sigma_b^3} \tag{52}$$

$$F_b(R_b, \varphi) = \frac{e^{-2R_b}}{R_b^2} \left(\frac{\cos^2 \varphi}{4} + \frac{\sin^2 \varphi}{R_b^2} \right). \tag{53}$$

Because these calculations are for radiation near the bottom, it will be assumed that atmospheric noise is smaller than system noise, and Eq. 29 will be used for $N(\omega)$. In figure 6, the function F_b is plotted as a function of R_b for $\varphi = 0, \pi/2$. G_b is also plotted as a function of f_0 for $TPI = 10^{-4}$ W sec m, $\sigma_w = 4$ mho/m, and $\sigma_b = 0.1$ mho/m. As in figures 4 and 5, the range at frequency f_0 can be obtained by finding the R_b for which $G_b(f_0) = F_b(R_b)$. The range in units of the bottom attenuation length, δ_b, is $R_b = r/\delta_b$. The range in meters can be obtained by using figure 1. Table 3 is a summary of the ranges obtained at the bottom for depths below those in figure 2 where the system noise limits the range.

Table 3. Summary of Ranges Obtained at the Bottom

Frequency (f), Hz	φ	R	Range, m
4	$\pi/2$	14	11,200
4	0	18	14,400
10	$\pi/2$	15.8	8,200
10	0	20	10,400
100	$\pi/2$	17.8	2,850
100	0	21	3,360

CONCLUSIONS

The results of calculations in the deep ocean, near the surface, and on the bottom are summarized in Chart 4, Section I. These ranges are those predicted for the assumed parameters under the best possible conditions. Parametric representations which can be used to predict range for other parameters are also given.

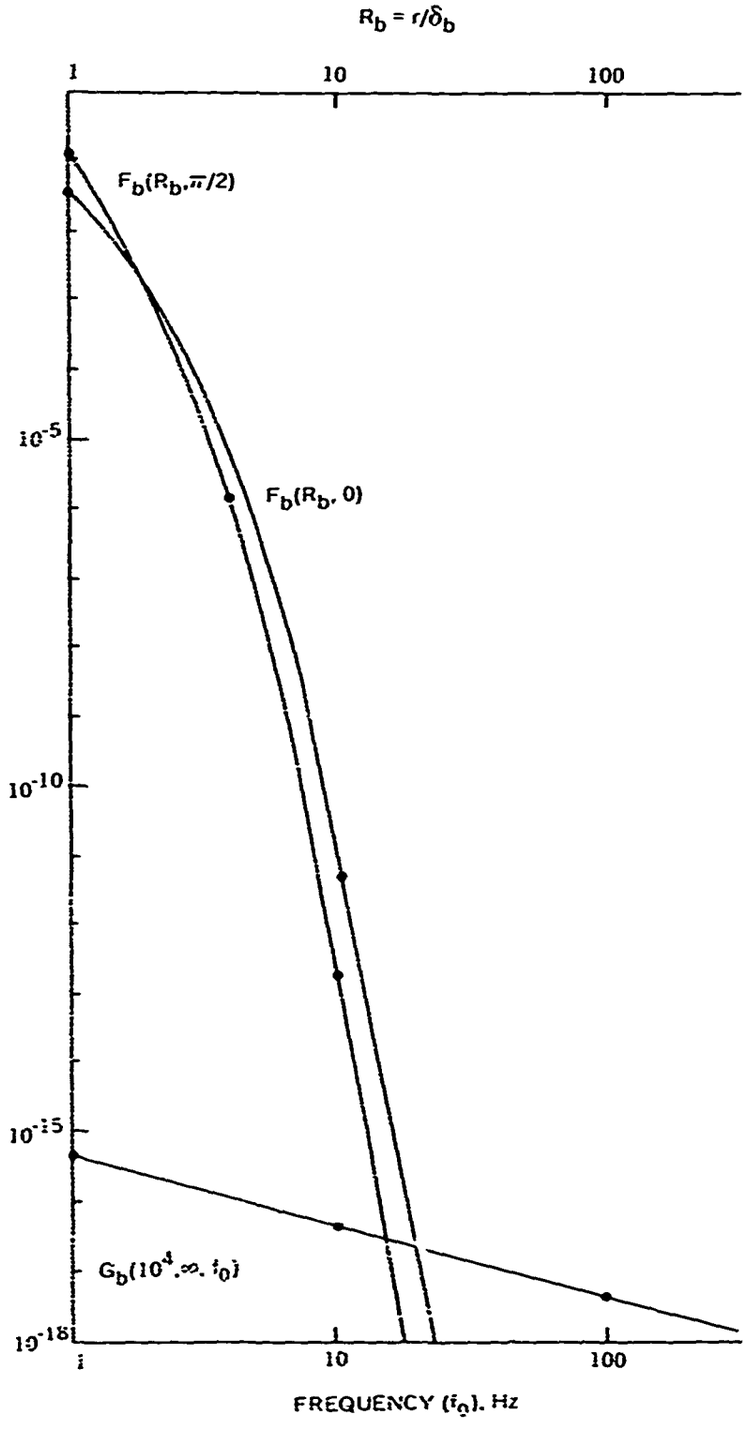

Figure 6. Functions $F_b(R,\varphi)$ and $G_b(TPI, h, f_0)$ for propagation at the bottom.

These results show the following characteristics.

1. The longest ranges are obtained for propagation near the surface where the wave propagates unattenuated through the air.

2. In the deep ocean, the range is longer near the bottom where propagation undergoes less attenuation. This calculation is sensitive to the local value of the bottom conductivity.

3. In the ocean far from the bottom, the greatest ranges are obtained at low frequencies and deep depths where atmospheric noise is greatly attenuated.

REFERENCES

1. M. B. Kraichman. *Handbook of Electromagnetic Propagation in Conducting Media.* pp. 2-1, A-2, 3-2, 3-16. U. S. Government Printing Office, Washington, D. C., 1970.

2. R. K. Moore. *Theory of Radio Communication Between Submerged Submarines.* pp. 95, 132, 134, 141. Ph.D. Thesis, Cornell University, 1951.

3. C. W. Helstrom. *Statistical Theory of Signal Detection.* p. 121. Pergamon Press, 1968.

4. E. F. Soderberg and M. Finkle. Electromagnetics in the Sea. *AGARD Conference Proc. No. 77.* 1970.

5. *American Institute of Physics Handbook.* pp. 6–200. McGraw-Hill Book Company, New York. 1963.

6. A. Baños and J. P. Wesley. *The Horizontal Electric Dipole in a Conducting Half Space.* Scripps Institute of Oceanography Reference 53-33, 1953.

UNDERWATER PROPAGATION OF LIGHT

by

A. Gordon
NUC

CONTENTS

UNDERWATER PROPAGATION OF LIGHT

INTRODUCTION

Increased absorption (wavelength dependent) and scattering by water and its particulate and dissolved impurities differentiate the visibility problems encountered underwater from those encountered in the atmosphere. Much information on the effects of water's absorption and scattering on image degradation is available (refs. 1 and 2). Within the present state-of-the-art, analytic results are available where the distance from the object to the observation point is small; however, at distances which are large compared with a scattering length, one is often forced to use the Monte Carlo ray-tracing methods.

The present article is concerned only with determining the maximum detection range of an underwater light source. This maximum detection range will place an upper bound on the distance obtainable in underwater viewing and the maximum operating distance of a light-based detection, navigation, or communication system.

In the following portions of this article, we will consider various light sources and show that lasers appear to be most efficient for producing maximum on-axis illumination. The detection of light will be shown to be limited by the requirement that approximately 10 photons reach our detector in the required time interval. Calculations will then be made assuming first distilled water and then clearest ocean water for the case of no background illumination. Finally, it will be shown that, for depths less than approximately 4000 m, both bioluminescence and daylight filtering in from the surface further limit the maximum attainable range.

SOURCES

Three types of sources, which appear most applicable to the underwater environment, will be considered. The first two are lasers which have their power concentrated in wavelengths within the region of water's greatest optical transmission, i.e., between 4500 and 5500 Å. The characteristics of these lasers, the neodymium-doped frequency-doubled yttrium-aluminum-garnet (Nd:YAG) laser and the argon laser, are listed in table 1. The characteristics listed for the YAG laser are better than the state-of-the-art, and assume the near-term solution of the collimation-conversion problem. The most significant differences between the two lasers are listed below.

1. The availability of energy near 4750 Å, which is often the wavelength of least attenuation by clearest ocean water, for the argon laser.
2. The large peak powers available in the YAG laser.

The latter difference becomes important when strong background flux limits the range of the laser. Both lasers have a similar total output: 5 J/sec for the YAG laser and 10 J/sec for the argon laser. These lasers also have the advantage of a high degree of collimation, but the offsetting disadvantage of low efficiency.

The third source, a thallium-iodide (TlI) doped mercury arc lamp, offers the advantage of a high efficiency output between 4500 and 5500 Å, but it has a low inherent collimation.

Table 1. Laser Characteristics.

Type	System Efficiency, percent	Peak Output Power, W	Repetition Rate, pps	Percentage of Output Power Distribution	Wavelength Uncertainty, Å	Pulse Duration	Beam Divergence (Spot Size)
Frequency-doubled YAG	1 to 2	5×10^6	100	100 percent -- 5300 Å	~20	10×10^{-9} sec	0.9×10^{-3} rad (2.5 mm)
Argon ion	0.1	10		10 percent -- 4765 Å 40 percent 4880 Å 40 percent - 5145 Å	0.01	continuous	0.9×10^{-3} rad (2.5 mm)

Efficiencies of 16 percent have been reported (ref. 3) for TlI doped mercury lights, and the lamps have been constructed, with a reduced efficiency, with arcs as short as 1 mm (ref. 4). For comparison purposes, the availability of a TlI doped mercury lamp with an efficiency of 16 percent and an arc length of 1 mm will be assumed.

A comparison between the on-axis illumination of the TlI doped mercury lamp and the argon laser can easily be made for their in-air performance. At a distance R from either source, the on-axis irradiance, H, will be approximately given by

$$H = \frac{PE}{\pi R^2 \theta^2} , \tag{1}$$

where P is the source's input power, E is the efficiency, and θ is the divergence half-angle. By inserting a two-lens collimator in front of the laser's output, θ becomes

$$\theta = \frac{A_1}{A_2} \theta_i , \tag{2}$$

where A_1 is the diameter of the entrance pupil, A_2 is the diameter of the exit pupil, and θ_i is the initial divergence angle. For the TlI doped mercury lamp placed in front of a parabolic reflector, we obtain a beam divergence half-angle of

$$\theta = \frac{l}{R_A} , \tag{3}$$

where l is the length of the lamp's arc and R_A is the radius of the reflector. Inserting Eqs. 2 and 3 and using the ratio of the laser's illumination, H_L, to that of the TlI source, H_{TlI}, we have

$$\frac{H_L}{H_{TlI}} = \frac{E_L}{E_{TlI}} \frac{4 l^2}{\theta_i^2 A_1^2} , \tag{4}$$

where we have assumed equal power inputs and equal exit pupils. Inserting the values $E_L = 10^{-3}$, $E_{TlI} = 0.16$, $l = 1$ mm, $\theta_i = 0.45 \times 10^{-3}$, and $A_1 = 2.5$ mm, we obtain $H_L = 2 \times 10^{-4} H_{TlI}$.

The illumination in the forward direction in air is then 2×10^{-4} times greater than that produced by the TlI lamp. In water, however, this ratio will not be as great because of multiple scattering effects. These effects affect the laser and TlI beam differently because the TlI beam will have a larger divergence angle and a greater proportion of the scattered flux will not be scattered out of the beam for equally sized optics. This means that the effective coefficient, α_{eff}, will be closer to the true attenuation coefficient for the laser than for the TlI bulb. This, in turn, implies that the on-axis illumination will be attenuated more rapidly for the laser. Because of the lack of measurements or Monte Carlo data for the distances in which we are interested, this discussion will be confined to the lasers listed in table 1. It will be assumed

that these lasers are terminated in a 1-in. collimator so that the beam divergence half-angle is 0.45×10^{-4} rad. In the next section, an argument will be given to show that at the ranges and observation angles of interest, the laser beam is attenuated as $e^{-\alpha R}$, where α is the true attenuation coefficient.

RANGE IN DISTILLED WATER

In this section, we will calculate the range of the lasers through distilled water, which must, of necessity, be an upper bound to ranges obtainable in natural water. It has been shown that filtered natural water, however, behaves like distilled water (ref. 5). In this discussion, the data of Clarke and James will be considered as representative of distilled water's attenuation. It will be also assumed that the detector is capable of detecting single photons (this will be discussed in the next section). For the present calculations, 5 sec will be the decision time, i.e., it will be required that the mean photon arrival rate be 0.2 photons/sec.

A beam with an initial circular beamwidth radius, r_1, and a half-divergence angle, θ, will produce in air a spot of size $r \cong \sqrt{R^2\theta^2 + r_1^2}$ at a distance R from the source. If F_0 is the flux emitted by the light source, the on-axis intensity will be given by

$$H = \frac{F_0}{\pi(R^2\theta^2 + r_1^2)} . \tag{5}$$

Using a receiver with an aperture of radius r_2, the total flux collected in t sec will be

$$F = \frac{F_0 r_2^2 t}{R^2\theta^2 + r_1^2} . \tag{6}$$

The above formula is somewhat erroneous when the spot size is smaller than the receiver aperture; however, with the similarly sized optics used in this article, this error is negligible.

Because of scattering and absorption losses, the flux in water is less than the value given in Eq. 6, and because of multiple scattering effects, it has yet to be determined whether the beam is exponentially attenuated by the product of the range and the true attenuation coefficient. Duntley (ref. 6) has done some work on this problem. His figure 5 is plotted in different form as figure 1 in this article. The ordinate is the solid angle subtended by the receiver divided by 2π, and the abscissa is the range in attenuation lengths for which using the true attenuation coefficient gives a wrong answer by a factor of 10. The narrower the field-of-view, the longer the range for which the use of the true attenuation coefficient is justified. Using a straight-line extrapolation through the last two points of figure 1 and using the present beam divergence solid angle $\Omega/2\pi = 1.01 \times 10^{-9}$, we find that the use of the true attenuation coefficient is justified to a range of approximately 34 attenuation lengths. For our calculations, we expect the true attenuation coefficient to be valid over a somewhat greater range for the following reasons.

1. We used a linear extrapolation of figure 1, whereas the actual curve exhibits upward curvature.

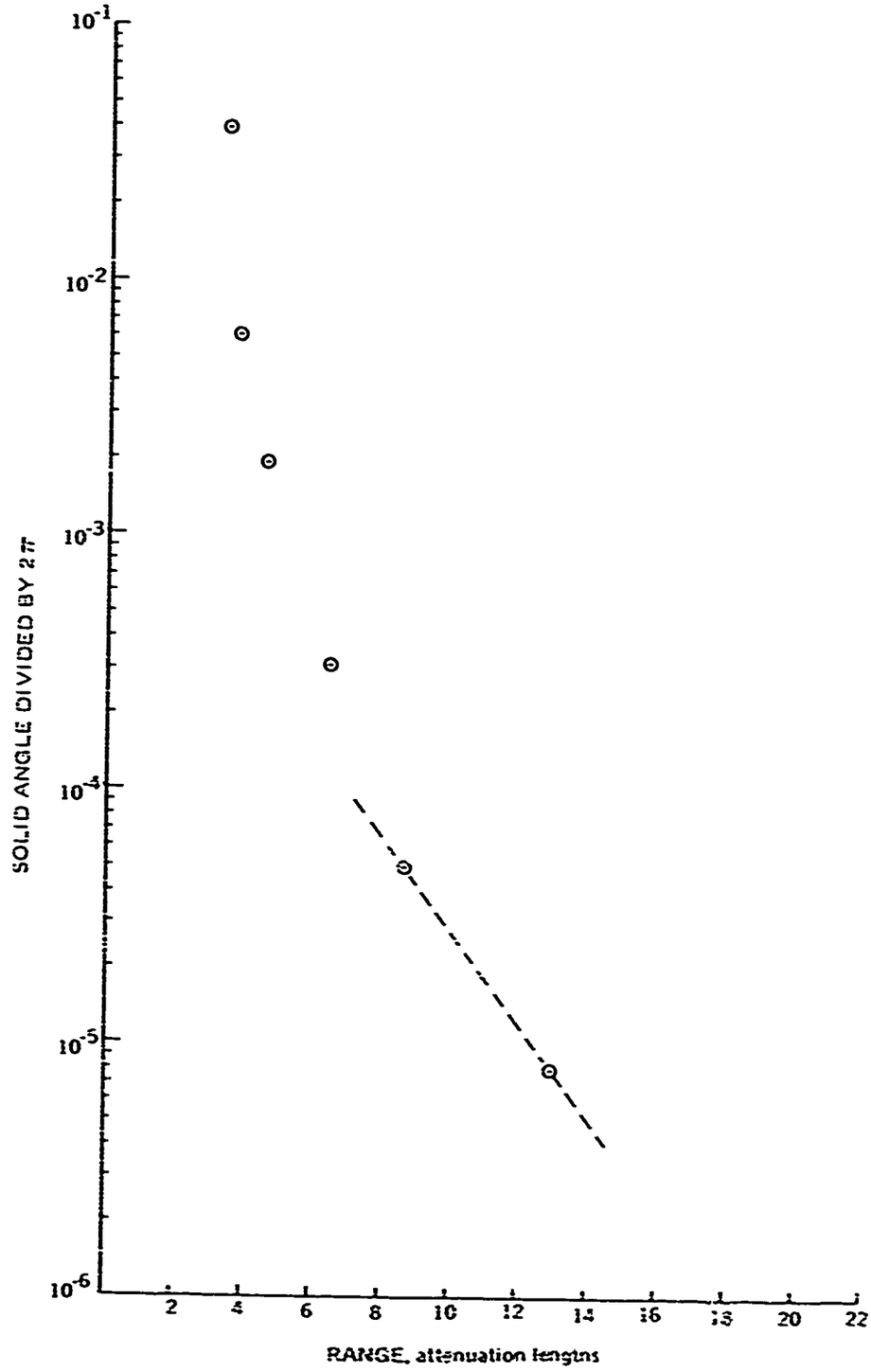

Figure 1. The range at which the use of the attenuation coefficient results in an error of 10 in received flux.

2. The waters which are used in this article have a lower scattering-to-absorption ratio than that reported by Duntley.

Because of these factors, the total flux intercepted in water will be given by

$$F = \frac{F_0 r_2^2 t e^{-\alpha R}}{(R^2 \theta^2 + r_1^2)}. \qquad (7)$$

Throughout the rest of this article, t = 5 sec, $\theta = 4.5 \times 10^{-5}$ rad, and $r_2 = 1.0$ in.

For distilled water, the data of Clarke and James shows that for the argon ion laser $\alpha = 0.019$/m at 4765 Å and $\alpha = 0.047$/m at 5300 Å for the frequency-doubled YAG laser. In the 5-sec observation time, the photon flux, F_0T, is 1.2×10^{19} photons for the 4765-Å line of the argon ion laser and 6.68×10^{19} photons for the frequency-doubled YAG. Inserting these values in Eq. 7 and requiring that F = 1 photon in the 5-sec observation interval, we find that the range of the argon laser is 2170 m and the range of the YAG laser is 947 m. The next section will show that the ranges actually obtainable in the ocean environment are less than those calculated for distilled water.

DETECTORS

Photomultiplier tubes are among the most sensitive detectors of light in the visible region. One disadvantage of these detectors is the "dark noise," i.e., the output current observed at the photomultiplier anode in the absence of any light input. In high quality photomultipliers, the dark current can be reduced by cooling. For example, data on the RCA type 1P21 shows that the photocathode dark-current emission is approximately one photoelectron per sec at -150 °C (ref. 7). Because the residual dark current after cooling mainly consists of multiple electron pulses while the signal at low light levels is mainly single electron pulses, the noise can be additionally reduced by passing the output of the photomultiplier through a pulse-height discriminator. Due to the small value of the dark current after cooling and the possibility of discrimination against the remaining dark current, we will neglect the photomultiplier dark current in the calculations.

One source of noise which must be considered for any realistic laser-range calculation is the noise associated with the statistical distribution of the photon arrival times. For a Poisson distribution, the distribution of photoelectrons will also be Poisson (ref 8) with a mean emission rate equal to the quantum efficiency of the photocathode times the photon arrival rate. In the portion of the spectrum in which we are interested, a typical value for the quantum efficiency is 20 percent. To have a 90 percent probability of at least one photoelectron being emitted during the observation interval, a mean photoelectron emission rate of 2.3 photoelectrons or a photon arrival rate of 11.5 photons is required during the observation interval. Thus, a value of 11.5 will be used for F in Eq. 7 in the calculations in the next section.

RANGE IN CLEAREST OCEAN WATER

In addition to the attenuation produced by distilled water, ocean water contains particulate matter and dissolved organic substances which contribute to the total scattering and absorption. Burt (ref. 9) has taken extensive data in the tropical Pacific on the variation of beam attenuation with wavelength, depth, and location. For the present calculations, we will use

his data for the clearest water he observed. This water, found at 450 m, has a transmittance relative to distilled water which rises from 98 percent at 4500 Å to 99 percent at 5500 Å. Burt's clearest water is thus slightly clearer than the 98 percent transmission for low ocean water given by Sverdrup, Johnson, and Fleming (ref. 10). Using Burt's clearest water, we obtain attenuation coefficients of $\alpha = 0.039$ for the 4765-Å line of the argon laser and $\alpha = 0.06$ for the 5300-Å output of the YAG laser. Inserting these values into Eq. 7, we obtain a range of 1030 m for the argon laser and 710 m for the frequency-doubled YAG laser. These ranges were calculated on the basis of no background illumination. The effect of a light background is discussed in the next section.

RANGE IN THE PRESENCE OF BACKGROUND FLUX

Ambient background flux makes the decision concerning the presence of the laser more difficult, thus reducing the range below that given in the last section. The sources of background illumination are blackbody radiation of the water medium, skylight which penetrates to the laser's operating depth, and bioluminescence.

The total number of photons per unit area, per unit wavelength per second, emitted by a blackbody can be expressed as (ref. 11)

$$N_\lambda = \frac{2\pi c}{\lambda^4 (e^{\epsilon/kT} - 1)} , \tag{8}$$

where c is the velocity of light = 3×10^{10} cm/sec, $\lambda = 5300$ Å $= 5.3 \times 10^{-5}$ cm, ϵ is the energy of a 5300-Å photon = 2.34 eV, and kT = 1/40 eV at room temperature. Inserting these values in Eq. 8, we find $N_\lambda = 5.34 \times 10^{-3}$ photons/sec cm^3. Using a detector area of $\pi(1 \text{ in.})^2 = 20.3$ cm^2 and a 100 Å $= 10^{-6}$ cm acceptance band, we find a photon flux due to blackbody radiation of 1.08×10^{-17} photons per second. This flux is extremely small; thus, the photon flux caused by blackbody radiation is completely negligible.

Clarke and Denton (ref. 12) give a schematic diagram for the penetration of light into the sea. Their figures are for a clear sunny day and for the clearest ocean water (diffuse attenuation coefficient = 0.033/m). Their data will be used assuming a constant spectral distribution of flux in the region between 4500 and 5500 Å and neglecting orientation effects. In using data for brightest daylight, we will be considering the maximum possible limitation on range due to penetration of surface light. This limitation extends to about 650 m, at which depth bioluminescence becomes the dominant background.

Bioluminescence is the major source of background light at all depths on dark nights and at depths below about 650 m (the latter is valid even on the brightest days in the clearest water). The extensive data in reference 12 shows that illumination due to bioluminescence has average values of 10^{-5} μW/cm^2 at 650 m to about 10^{-9} μW/cm^2 at 3750 m. Bioluminescent activity thus decreases with depth, but not necessarily monotonically. The maximum bioluminescence observed at any depth greater than 650 m, however, does not appear to exceed 10^{-5} μW/cm^2.

For the detection of the laser beam in the presence of background illumination, coherent detection will be assumed. This type of detection yields the greatest signal-to-noise level, thus placing an upper bound on the range for a given source power and background

illumination. Coherent detection can be accomplished by feeding the output of the photomultiplier into a noiseless (i.e., cooled) load resistor and using the voltage across the resistor as the input to the matched filter.

Current noise in the photomultiplier tube causes a white spectral noise density, $\phi(\omega)$, equal to

$$\phi(\omega) = \mu^2 e \bar{i} \ . \tag{9}$$

where μ is the photomultiplier gain, e is the electronic charge, and $\bar{i}$ is the time-averaged photocathode current which is equal to

$$\bar{i} = \bar{i}_s + \bar{i}_n \ . \tag{10}$$

where $\bar{i}_s$ and $\bar{i}_n$ are the time-averaged laser and background photocathode currents, respectively.

The instantaneous signal anode current, i_s, is given by

$$i_s = F\mu\eta e \ . \tag{11}$$

where η is the quantum efficiency ($\eta = 0.2$). F is given by Eq. 7 except that $F_0 t$ is replaced by F_0', the instantaneous source flux ($F_0' = 1.5 \times 10^{25}$ photons/sec for the YAG laser and 2.41×10^{18} photons/sec for the argon laser). The instantaneous anode current due to background is

$$i_n = HA\tau p\eta\mu e \ , \tag{12}$$

where H is the background illumination in W/cm^2; A is the detector area (A = 20.3 cm^2); p is the number of photons/sec/W (2.41×10^{18} photon/sec/W at 4765 Å and 2.67×10^{18} photon/sec/W at 5300 Å); and τ is the fraction of illumination that is passed through any narrowband filter which can be placed in front of the photomultiplier. Assuming a constant background illumination within the band 4500 to 5500 Å, an ideal 20-Å filter will yield $\tau = 0.2$.

Coherent detection in the presence of white noise is governed by the equation

$$d^2 = \frac{\int_0^T s^2 dt}{\phi(\omega)} \ , \tag{13}$$

where $s^2 = i_s^2$ for our case, T is the observation time, and d is the signal-to-noise ratio. We choose d = 2, which will yield a false alarm probability of 0.2 at a detection probability of 0.85. Substituting Eqs. 10, 11, and 12 in Eq. 9, we have

$$\phi(\omega) = \mu^2 e^2 \eta (MF + HA\tau p) \ . \tag{14}$$

where the factor M is 1 for the argon laser and 10^{-6} for the YAG laser. Substituting Eqs. 11 and 14 in Eq. 13, we find

$$d^2 = \frac{TMF^2\eta}{MF + HA\tau p} \quad . \tag{15}$$

Setting T equal to 5 sec leaves an equation for F, the flux entering the detector in terms of the background illumination H. Using the daylight penetration data of Clarke and Denton and the bioluminescence data of Clarke and Hubbard, appropriate values for the ambient background for a given depth can be found, and F at this depth can be determined. The range at this depth is determined by inserting the appropriate value of F into Eq. 7 and solving for R. α, assumed independent of depth, is 0.039/m for the argon laser and 0.06/m for the YAG laser as in the zero background calculations in the last section.

RESULTS AND DISCUSSION

The variation of maximum laser range with depth for bright daylight surface illumination is shown in figure 2 and Chart 5, Section I. At the deepest depths, the bioluminescence and daylight penetration are too weak to limit the laser's range; thus, the range is photon limited. For the argon laser, the range is photon limited in depths over 4000 m, while the YAG laser retains the photon-limited range to 2500 m. The YAG laser is less affected primarily because its radiation is chopped, and the coherent detector is better at selecting this signal from the background than the cw output of the argon laser. At depths between 650 and 4000 m for the argon laser and at depths between 650 and 2500 for the YAG laser, the range is limited by bioluminescence. The 650-m upper limit for bioluminescence will become shallower at night when the flux penetrating the surface is less. Various points, plotted on figure 2 for the daylight-limited regime between 650 and 75 m, illustrate the difference between the argon and the YAG lasers. In this region, the range of the YAG laser again decreases more slowly because of coherent detection. Although figure 2 shows that the argon laser has a greater range at a 75-m depth, this is due to the use of $\alpha = 0.039$/m. The possibility of finding water with this clarity near the surface is remote, and a value of $\alpha \geq 0.06$/m is more appropriate. In this case, the near-surface daylight range of the YAG laser will surpass that of the argon ion laser.

The calculations in this article show that laser ranges in excess of 1000 m in the ocean environment are difficult to obtain. To obtain detection ranges greater than those previously discussed, it is necessary to increase the power input, receiving aperture area, or observation time. For the photon-limited operation, an increase in any one of these by a factor of 10 increases the range by approximately 2 attenuation lengths; 2 attenuation lengths are approximately 32 m for the YAG laser and 50 m for the argon laser. Thus, it appears that very little range will be gained by changing the system parameters used in this article.

The major limitation concerning the accuracy of the calculations in this article is the uncertainty concerning the correct attenuation coefficient to use on-axis at long distances. The maximum possible range of the effective attenuation coefficient is from a, the absorption coefficient of distilled water, to α, the attenuation coefficient. If a is the effective attenuation coefficient, the range in ocean water can be as large as the range for distilled water. Duntley's results (ref. 6), however show that attenuation coefficients

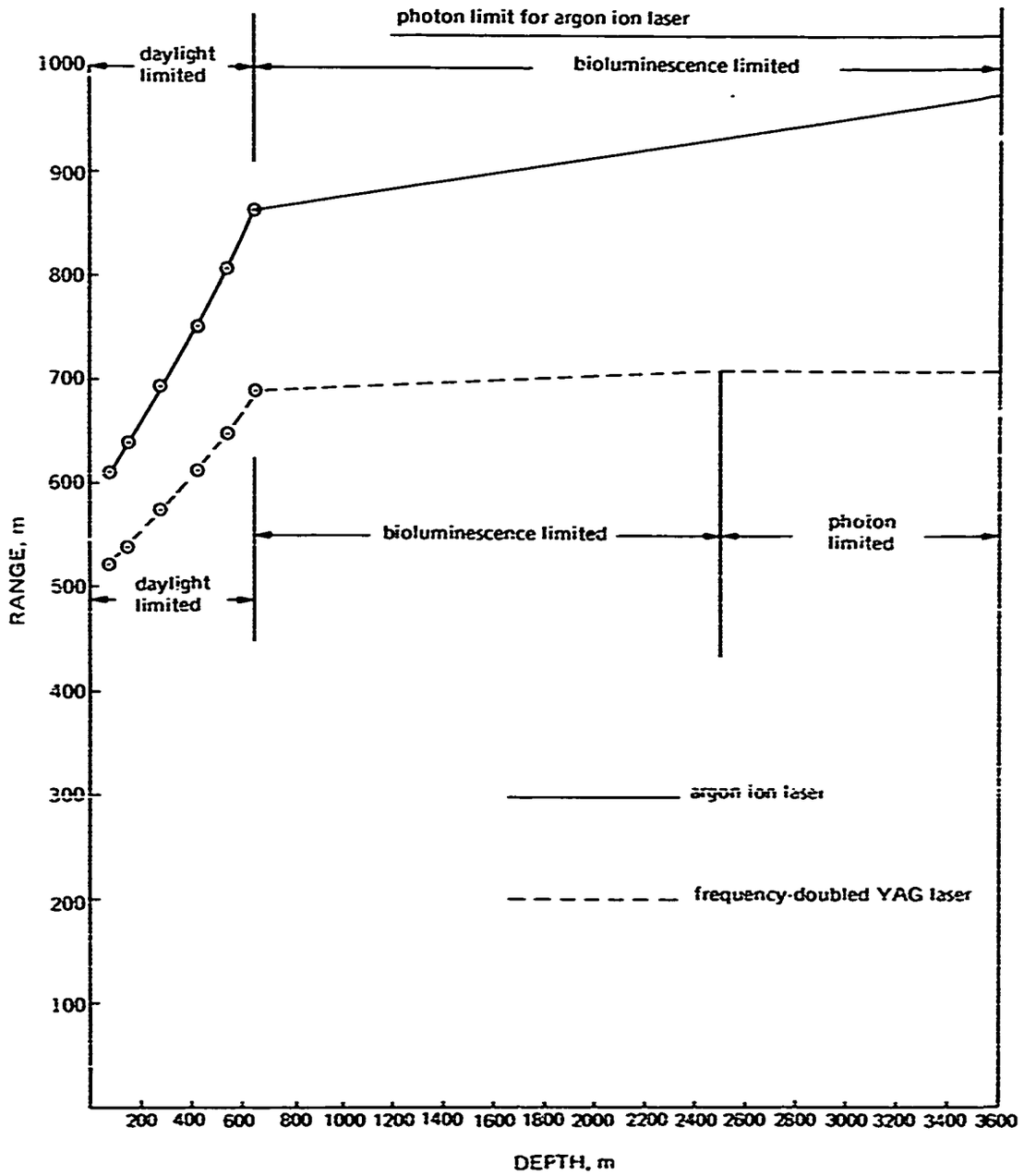

Figure 2. Laser performance as a function of depth.

used in the sections, *Range in Clearest Ocean Water* and *Range in the Presence of Background Flux*, are probably more accurate. The final determination as to the correct attenuation coefficient must come from some theoretical method, such as Monte Carlo methods or experimental measurements. Monte Carlo ray tracing is difficult at long ranges and for small receiver apertures. Duntley (ref. 6), however, indicated that it was possible for him to extend his small-angle measurements to at least 40 attenuation lengths. Based on the results of this article, such experiments are desirable.

REFERENCES

1. S. Q. Duntley. Light in the Sea. *Journal of the Optical Society of America.* v. 53, pp. 214–233, 1963.

2. N. G. Jerlov. *Optical Oceanography.* Elsevier Publishing Company, 1968.

3. A. R. Waltz. *A Study of Light Sources for Underwater Use.* p. 39. Naval Undersea Research and Development Center, NUC TP265, 1970.

4. M. Kerpchar and B. Lichtenstein. *Preliminary Study for Illumination-Modulated, Synchronized Shutter Underwater TV System-Transmitter Parametric Design.* p. 23. Ocean Metrics, Inc., Fairfield, New Jersey, 1970.

5. G. L. Clarke and H. R. James. Laboratory Analysis of the Selective Absorption of Light by Seawater. *J. Opt. Soc. Amer.* v. 29, pp. 43–55, 1939.

6. S. Q. Duntley. *Underwater Optics.* University of California, La Jolla, California, letter report A AD 647791, 1966.

7. RCA Corporation. *RCA Photomultiplier Manual.* p. 44. RCA Electronic Components, Harrison, N. J., 1970.

8. D. L. Fried. Noise in Photomission Current. *Applied Optics.* pp. 79–80, January 1965.

9. W. V. Burt. Selective Transmission of Light in Tropical Pacific Waters. *Deep Sea Research.* v. 5, pp. 51–61, 1958.

10. H. U. Sverdrup, M. W. Johnson, and R. H. Fleming. *The Oceans.* Prentice-Hall, Inc., New York, 1946.

11. *Electro-Optics Handbook.* p. 4-1. Radio Corporation of America, Burlington, Mass., 1968.

12. G. L. Clarke and E. J. Denton. Light and Animal Life in *The Sea*, M. N. Hill, ed. v. 2, pp. 456–468. Interscience Publishers, New York, 1962.

13. C. W. Helstrom. *Statistical Theory of Signal Detection.* p. 106. Pergamon Press, New York, 1968.

ACOUSTIC TRANSPONDERS FOR NAVIGATION REFERENCE POINTS

by

C. D. Lowenstein
Marine Physical Laboratory
Scripps Institute of Oceanography

CONTENTS

ACOUSTIC TRANSPONDERS FOR NAVIGATION REFERENCE POINTS

INTRODUCTION

The prominent use of acoustics in the underwater environment is due to the ability of sound to be propagated over long distances and, at the same time, to carry a substantial amount of information. Sound is used in underwater communication, control, detection, and navigation. The present article will examine the range, power, and frequency tradeoffs in an acoustic transponder navigation system using pulse-burst signals.

TRANSPONDER CONSIDERATIONS

An acoustic transponder is a device which replies with an acoustic signal when it is interrogated with an acoustic signal. The use of acoustic transponders in undersea navigation is based on the fact that the speed of sound in water is nearly constant and that it can be measured or calculated when necessary. Thus, the time needed for an interrogation signal to travel from the navigated vehicle to the transponder and for the reply signal to return to the vehicle is a direct measure of the range from the vehicle to the transponder. By a suitable choice of signal encoding, the interrogations and replies of several different transponders can be distinguished, allowing the use of several independent reference points in a navigation system.

Because acoustic interrogation follows the same path as a transponder reply and because the two signals normally use adjacent frequency bands, this analysis will consider only the one-way travel path. It is assumed that the construction of both the transponder and interrogator are similar, e.g., receiver sensitivity, transmitter power output, and transducer size.

Transmitted power is limited by the power density, which can be applied to the transmitting transducer, to no more than 1 W/cm^2 near the surface. For this article, it has been assumed that the transmitting and receiving transducers are vertical cylinders that are 1 wavelength in diameter and length. Such a transducer has a 3-dB directional gain in the horizontal plane and a vertical beamwidth of 120 deg. The peak transmitted power is severely limited at high frequencies because the available area decreases as the square of the frequency.

The power consumption of a transponder is in two modes: listening power, perhaps 30 mW, and transmitting power, which will typically be approximately 0.2 percent of the peak transmitted power because of the limited duty cycle. Thus, the total power consumption of a transponder while it is in action will be 30 mW to 2 W.

The size of the transponder is primarily determined by the size of its battery pack because the size of the electronic components is much smaller than the batteries. Over the frequency range considered, the size of the transponder might be 15 cm x 15 cm x 1 m. The weight will be 10 to 50 kg, and the cost will be $2000 to $5000.

NOISE

The fundamental question in this section concerns the range at which a signal can be transmitted so that it can be recognized above the background noise at the other end of the path. If this is the interrogation signal, the transponder must recognize its interrogation to generate a reply. Similarly, the receiving apparatus at the vehicle must recognize the reply from the transponder to measure the acoustic travel time and thus to measure the range to the transponder. The assumption will be made that the signal energy in the received band must be at least 10 dB greater than the background noise in the same band.

In the general frequency range of interest (10 kHz to 1 MHz), there are two noise mechanisms. Up to approximately 30 kHz, the dominant noise, decreasing with increasing frequency, is generated by wave motion at the sea surface; above 30 kHz, thermal noise, increasing with increasing frequency, is dominant. The noise energy produced in the receiver will be proportional to the spectrum level of the external noise and to the receiver bandwidth. The receiver bandwidth should be matched to the bandwidth of the signal and hence to the length of the signal and the range resolution of the system.

CALCULATION OF SIGNAL RANGE

The signal energy available at the receiver will depend on the strength of the transmitted signal and on the loss which the signal undergoes during its travel through the water. The decibel loss of the signal as it passes from the transmitter to the receiver is a function of only the medium and the range; it is given by

$$\text{transmission loss} = 20 \log R + \alpha R , \tag{1}$$

where α is the (frequency dependent) attenuation coefficient and R is the range. The allowable transmission loss is given by

$$\begin{aligned} \text{allowable transmission loss} &= 71.6 + 10 \log \text{source power} \\ &+ \text{directivity index (source)} \\ &+ \text{directivity index (receiver)} \\ &- 10 \log \text{bandwidth} \\ &- \text{noise level} - \text{recognition differential} , \end{aligned} \tag{2}$$

where 71.6 is a unit conversion factor. The source power is determined by the transducer's area, proportional to the wavelength squared, and the cavitation limit of 1 W/cm^2. For the transducers used in this article, the directivity index is 3 dB for both the source and the receiver. A recognition differential of 10 dB is used, and the noise levels at various frequencies are given in Chart 6, Section I. For the present calculations, the resolutions are 1 m at 10 kHz and 0.1 m at 1000 kHz. The resolutions used for the higher frequencies are considerably lower than the maximum resolution; however, in the present calculation, resolution at the high frequency is sacrificed for an increased pulselength which lowers the bandwidth; this, in turn, lowers the background noise and increases the range. By inserting the appropriate values in Eqs. 1 and 2 and equating them, the maximum range is obtained.

RESULTS

Chart 6 of Section I illustrates the variation of maximum range with frequency. The large decrease in range with increasing frequency is due mainly to the rapid rise in the acoustic attenuation coefficient. The favorable range-bandwidth characteristics are evident, especially at frequencies of 100 kHz and below.

Figure 1 indicates the possible variation of maximum range with allowable transmission loss. A 10-dB degradation of allowable loss is possible because the ambient noise level is higher than the assumed threshold; however, 10-dB improvements are possible by using directive transducers and signal processing to increase the effective transmitted power.

BIBLIOGRAPHY

J. W. Horton. *Fundamentals of Sonar.* chapters 2-C and 3-A. U. S. Naval Institute, 1959.

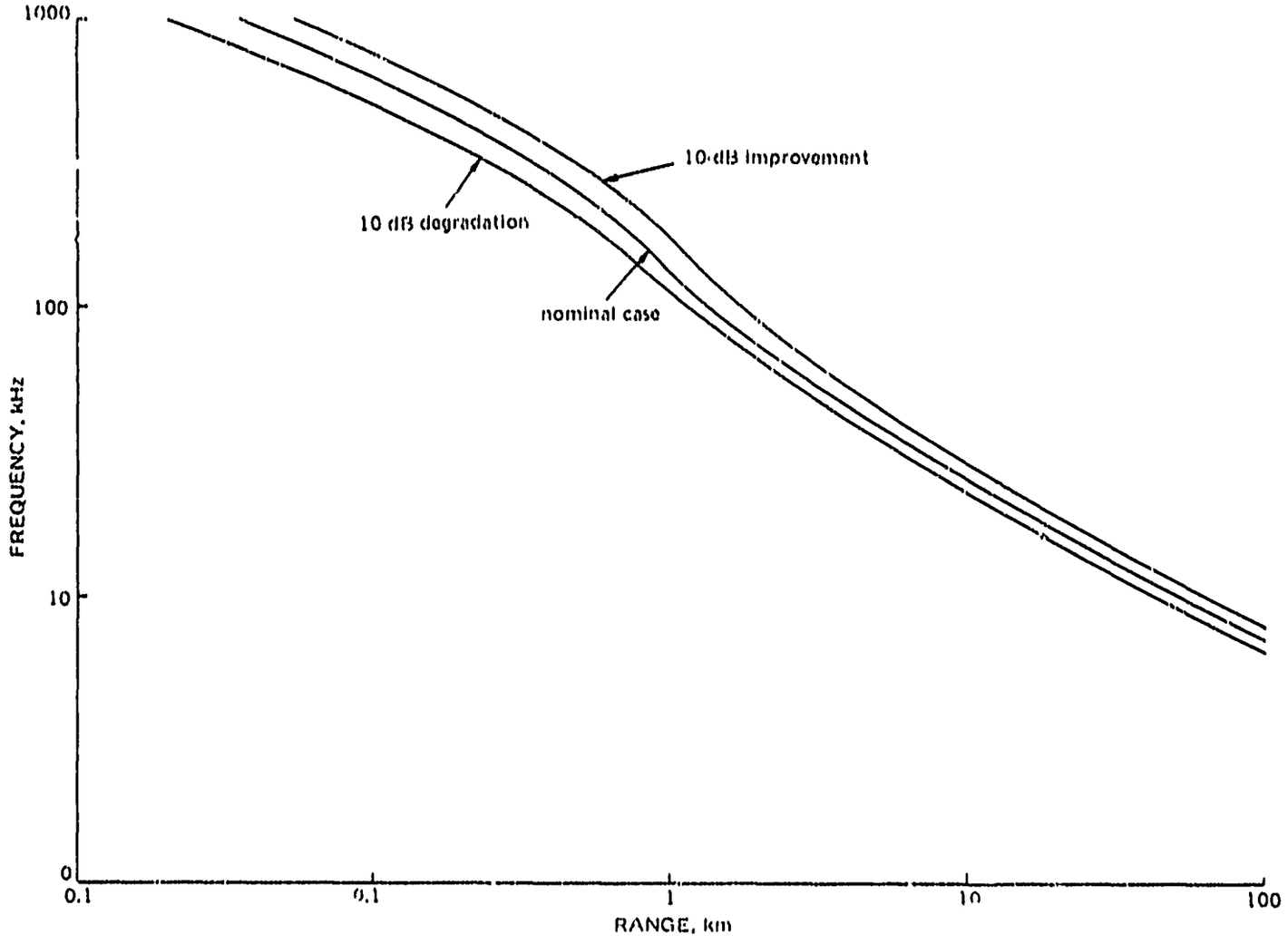

Figure 1. Acoustic transponder's achievable range.

MECHANICAL METHODS FOR DEEP SUBMERGENCE NAVIGATION

by

K. V. MacKenzie
NUC

CONTENTS

MECHANICAL METHODS FOR DEEP SUBMERGENCE NAVIGATION

INTRODUCTION

Although mechanical navigation aids, the first to be developed, are not the best or most versatile means of navigating in the deep ocean, they are simple, economical, and reliable, and if they are combined with dead-reckoning methods, a useful navigation system can be produced.

This article will describe some of the mechanical navigation aids that have been used aboard deep submergence vehicles such as the bathyscaph TRIESTE (refs. 1 through 6).

EXAMPLES OF MECHANICAL AIDS

Plastic Markers

In 1963, TRIESTE was used in the search for the nuclear submarine USS THRESHER, which disappeared in approximately 8500 ft of water 260 mi off the New England Coast. At this time, TRIESTE was the only Navy submersible capable of operating at such a depth.

One of the first navigational difficulties TRIESTE encountered was locating useful landmarks on the seafloor. A method that proved fairly satisfactory used 1441 plastic reference markers which were placed every 58 ft as an 11-line grid. The markers were numbered from 1 at the south end to 131 at the north, and each line was approximately 750 ft apart in the east-west direction (fig. 1).

The markers, tied to 10-lb sash weights, were dropped from an auxiliary ocean tug every 6 sec. The tug used Decca purple and green lines to control the track. Because neither the track nor the logistics of spacing could be held constant at the surface and because each marker took approximately 1 hr to reach the bottom, the effects of variable currents considerably distorted the actual landings. These "fortune cookies,"* however, were effective in identifying the various debris of the THRESHER, although 2 hr sometimes passed between sightings of markers.

On one dive, after initiating her descent with Decca data supplied by the support ship, TRIESTE descended outside the grid line and proceeded on a fixed course away from the grid because no markers were sighted. Thus, although the grid was approximately 1½-mi square, it was not large enough to allow for error in position at the surface or for lateral movement during descent.

In 1964, a second set of plastic markers, which could always be read, was dropped in the same area. Both sets of markers and the THRESHER debris appeared in photographs taken by cameras rigged on the TRIESTE or towed by surface ships.

---

*These markers were called fortune cookies because they had to unroll before the message could be read, and many failed to open.

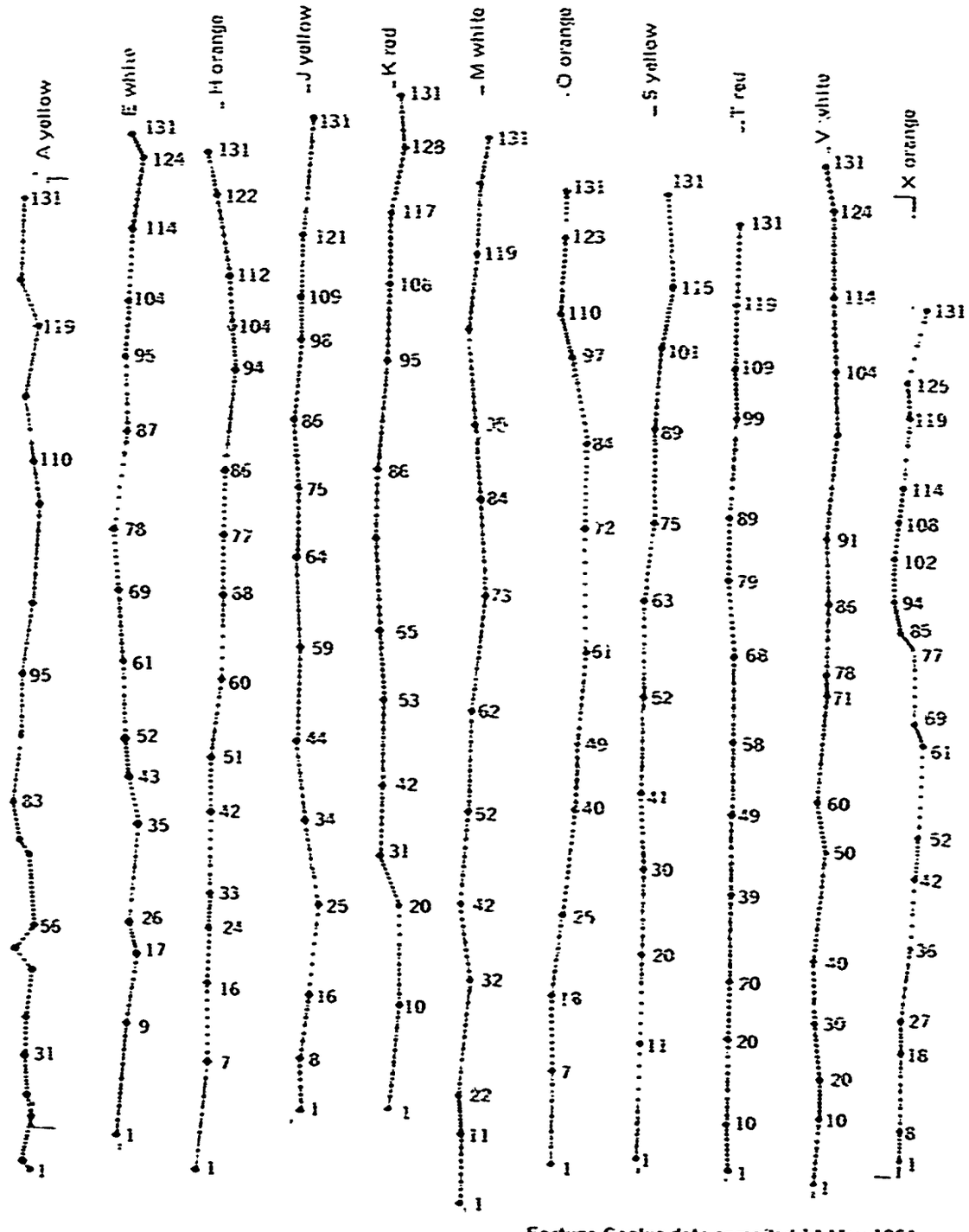

Figure 1. Plastic marker reference grid.

Reference Lines

Bottom reference lines that indicate position every 200 ft would be useful for submerged navigation. These lines would eliminate the possibility of passing between unsighted markers. The length of these lines should be at least two standard errors-of-estimate of surface-position accuracy, but not less than 1 mi in the open ocean.

For lines laid in an east-west direction, a vehicle could dive approximately 1 mi north of the estimated midpoint and proceed in a southern direction until the reference lines were sighted. It would then advance to a position indicator on the line to locate a reference point to initiate a controlled search.

The reference points would ideally be indicated by acoustic/optical reflectors moored approximately 10 ft above the bottom. The points could also be indicated by pingers, flashing lights, or transponders that reply only when queried with a proper code or frequency.

Unless prohibited by the nature of the operation, reference lines could be laid by a surface vessel or aircraft. Small anchors would be attached to marker points to hold the line in place on the seafloor. The line, however, should be weak enough to break, if fouled, without disturbing adjacent sections.

If surface ships or aircraft could not be used to lay the line, it could be done by a submersible. A method would have to be devised, however, for a submersible to lay a neutrally buoyant or slightly negatively buoyant line sporting periodic, anchored-moored, reference points. If each reference point had a net negative buoyancy of 15 lb, the submersible would become positively buoyant by that amount for each point laid. A 5000-ft line with markers every 200 ft would cause a buoyancy of 375 lb for the submersible, a buoyancy requiring compensation.

Reference Grooves

Reference grooves can be made by furrowing a line on the ocean floor with a specially designed tool. Markers can then be dropped into the furrow at regular intervals. These markers would probably remain in place because there would be no attached lines to drag them out of position. They could also be lighter than other markers because a negative buoyancy of 2 lb would probably keep them in place.

TRIESTE plowed grooves on the seafloor by dragging a 350-lb lead ball which was attached aft by a short line for control. The ball left a definite groove wherever it was dragged except on certain rock-strewn surfaces. The only problem the TRIESTE encountered was drag on slopes; at these instances, the work proceeded more slowly. Some trails made during the 1963 operations were still detectable in 1964, and more recent photographs from MIZAR show that some of the bottom marks have lasted well beyond the short time they were needed and used.

On some sea-floor terrain, such as the rock-strewn bottom encountered in the THRESHER search, scribed or scored grooves are largely ineffective. The trail is usually broken or obscured where gullies or large rocks appear, and movement or deposition of sediment near the shore will fill the grooves, limiting their effectiveness. This disadvantage can be overcome if nylon or other lines are used as adjuncts to the mark areas where plowing cannot be performed.

Wheel Devices

Devices which trail a wheel over the bottom have been used to measure the speed of advance, which, when coordinated with gyro headings in a small computer, yields a DR plot automatically. Accuracy, however, is limited where the bottom is gullied or where currents affect the vehicle and enter a component not sensed by the wheel.

The Perry Cubmarine tested a swiveled, weighted, bicycle wheel rim and fork that were rigidly connected to a 6-ft galvanized pipe (ref. 7). The distance traveled was recorded by a flexible cable-connected odometer. The total cost of the system was $19 75. Wheels. however, are not feasible aids in rocky terrain, on coral reefs, precipitous slopes, or sticky bottoms.

CONCLUSION

Relatively effective mechanical methods are available for deep submergence navigation, especially if they are augmented by acoustical, optical, and other attainable systems. Basic mechanical aids, however, can be used independently with competent results. If submersibles are designed with adequate cruising capabilities and means for ballast-loss compensation. they can lay reference lines and markers without surface assistance, thus simplifying the operation.

REFERENCES

1. K. V. MacKenzie. Sensors Installed on TRIESTE II in *Deep Ocean Search in the THRESHER Loss Area.* ONR-24. 1964.

2. K. V. MacKenzie. Bathyscaph TRIESTE Operations in the THRESHER Search. *U. S. Navy Journal of Underwater Acoustics.* v. 14. no. 2, pp. 301--304, April 1964.

3. K. V. MacKenzie. In Search of THRESHER in *Man Under Water* Underwater Society of America, Chilton Publishers, June 1965.

4. K. V. MacKenzie. Problems of Navigating on the Bottom of the Sea. *Naval Research Reviews.* v. 19, pp. 25–26, May 1966.

5. K. V. MacKenzie. Position Determination Under the Sea. *Transactions of Second Annual Marine Technology Society Conference and Exhibit: Exploiting the Ocean.* pp. 147–157, June 1966

6. K. V. MacKenzie. Early History of Deep Submergence Navigation Aboard TRIESTE. *Journal of the Institute of Navigation.* v. 17, no. 1, pp. 1–12, Spring 1970.

7. Roswell F. Busby and William F. Hart. Seafloor Navigation for Deep Submergence Vehicles. *Proceedings of Institute of Navigation National Marine Meeting. First Symposium on Manned Deep Submergence Vehicles* pp. 227–240, January 1966.

INITIAL DISTRIBUTION

1 Assistant Secretary of the Navy (R&D)
7 Chief of Naval Operations
- NOP-098T
- NOP-23
- NOP-90H
- NOP-942U
- NOP-967 (2)
- NOP981

2 Chief of Naval Material
- NMAT-034
- PM-7

4 Naval Air Systems Command
- NAIR-350
- NAIR-360
- NAIR-370
- NAIR-604

1 Naval Electronic Systems Command
- NELEX-0518

1 Naval Facilities Engineering Command (NFAC-03)
5 Naval Ordnance Systems Command
- NORD-03A
- NORD-03C
- NORD-05
- NORD-05121
- NORD-0632

3 Naval Ship Engineering Center
- NSEC-6142
- NSEC-6178C.03 (2)

11 Naval Ship Systems Command
- NSHP-03424
- NSHP-03542
- NSHP-065
- NSHP-2052
- PMS-395-00 (3)
- PMS-395-A2
- PMS-395-A4 (3)

5 Office of Naval Research
- Code 102-0S
- Code 104
- Code 466
- Code 480
- Code 485

4 Anti-Submarine Warfare Systems Project Office
    ASW-13
    ASW 14
    ASW-15
    ASW-22
1 Naval Air Development Center
1 Naval Civil Engineering Laboratory
2 Naval Coastal Systems Laboratory, Panama City
    Library
    Code 705
1 Naval Electronics Laboratory Center
1 Naval Missile Center
1 Naval Oceanographic Office (Code 9005)
3 Naval Ordnance Laboratory, White Oak
    Technical Library
    Code 212 (W. W. Taibert)
    Code 522 (N. Beck)
1 Naval Personnel Research and Development Laboratory
1 Naval Postgraduate School
3 Naval Research Laboratory
    Library
    Dr. Drummeter
    Dr. J. Elliot
2 Naval Ship Research and Development Center, Annapolis Division
    Library
    Code A723
2 Naval Ship Research and Development Center, Carderock Division
    Library
    Code H90
3 Naval Torpedo Station, Keyport
    Quality Evaluation and Engineering Laboratory, Technical Library
    Director, Research and Engineering
    Code 323
1 Naval Training Device Center
1 Naval Underwater Systems Center, New London Laboratory
1 Naval Underwater Systems Center, Newport Laboratory
1 Naval Weapons Center (Code 753)
1 Navy Space Systems Activity, SAMSO (Code 50)
1 Navy Underwater Sound Reference Laboratory, Orlando
1 Oceanographer of the Navy (ONC2)
1 Submarine Development Group ONE
1 Submarine Development Group TWO
2 Defense Documentation Center
1 Army Electronics Laboratories, Army Electronics Command, AMSEL-4L-CT-0
1 Army Engineer Research and Development Laboratories, Fort Belvoir (STWFO Branch)
1 Advanced Research Project Agency, Advanced Sensors Office, Advanced
    Engineering Office
1 Applied Physics Laboratory, University of Washington

1 Marine Physical Laboratory, Scripps Institution of Oceanography
1 Ordnance Research Laboratory, Pennsylvania State University
1 Oregon State University, Department of Oceanography, School of Science, Corvallis
2 Scripps Institution of Oceanography, University of California, Visibility Laboratory
R. W. Austin
S. Q. Duntley
1 Woods Hole Oceanographic Institution

Center Distribution:

01	1311(2)	35	6502	6512
0101	152	45	6504	652
02	153	50	6505	653
04	25	60	6506	654
051	2501	6005	651	96
131	2502	65	6511	9601

UNCLASSIFIED
Security Classification

DOCUMENT CONTROL DATA - R & D

Security classification of title, body of abstract and indexing annotation must be entered when the overall report is classified)

1 ORIGINATING ACTIVITY (Corporate author) Naval Undersea Research and Development Center San Diego, California 92132	2a. REPORT SECURITY CLASSIFICATION UNCLASSIFIED 2b. GROUP

3 REPORT TITLE

UNDERSEA DETECTION OF VARIOUS SIGNALS

4 DESCRIPTIVE NOTES (Type of report and inclusive dates)

Research and Development September 1970 to March 1971

5 AUTHOR(S) (First name, middle initial, last name)

A. Gordon, editor

6 REPORT DATE July 1972	7a. TOTAL NO OF PAGES 95	7b. NO OF REFS
8a CONTRACT OR GRANT NO b PROJECT NO S-1001, S-1001-001 c d	9a. ORIGINATOR'S REPORT NUMBER(S) NUC TP 294 9b. OTHER REPORT NO(S) (Any other numbers that may be assigned this report)	

10 DISTRIBUTION STATEMENT

Distribution limited to U.S. Government agencies only. Proprietary information, April 1971. Other requests for this document must be referred to the Naval Undersea Research and Development Center, San Diego, Calif. 92132.

11 SUPPLEMENTARY NOTES	12 SPONSORING MILITARY ACTIVITY Naval Ship Systems Command Washington, D. C. 20360

13 ABSTRACT

Tradeoffs involved in the undersea detection of static and time-varying signals are examined and the quantitative results are discussed in this report. Static electric and magnetic fields, radioactive fields, chemical systems, extremely-low-frequency (ELF) electromagnetic radiation, light, and acoustics were studied, and the results were tabulated in chart form. For time-varying fields, underwater light exhibits inferior range and ELF exhibits inferior bandwidth when compared with acoustics. Ranges from approximately 3 to 14 km are achievable for chemical and ELF sources, respectively, when they are used as static markers.

DD FORM NO. 1473 (PAGE 1)
(123-024-6614)

UNCLASSIFIED
Security Classification